© 2017. Published by The Company of Biologists Ltd | Development (2017) 144, 211-220 doi:10.1242/dev.142497

Endothelial cell regulation of salivary gland epithelial patterning

Hae Ryong Kwon[1,2,*], Deirdre A. Nelson[1], Kara A. DeSantis[1,2], Jennifer M. Morrissey[1,‡] and Melinda Larsen[1,§]

ABSTRACT

Perfusion-independent regulation of epithelial pattern formation by the vasculature during organ development and regeneration is of considerable interest for application in restoring organ function. During murine submandibular salivary gland development, the vasculature co-develops with the epithelium during branching morphogenesis; however, it is not known whether the vasculature has instructive effects on the epithelium. Using pharmacological inhibitors and siRNA knockdown in embryonic organ explants, we determined that VEGFR2-dependent signaling is required for salivary gland epithelial patterning. To test directly for a requirement for endothelial cells in instructive epithelial patterning, we developed a novel *ex vivo* cell fractionation/reconstitution assay. Immuno-depletion of CD31$^+$ endothelial cells in this assay confirmed a requirement for endothelial cells in epithelial patterning of the gland. Depletion of endothelial cells or inhibition of VEGFR2 signaling in organ explants caused an aberrant increase in cells expressing the ductal proteins K19 and K7, with a reduction in Kit$^+$ progenitor cells in the endbuds of reconstituted glands. Addition of exogenous endothelial cells to reconstituted glands restored epithelial patterning, as did supplementation with the endothelial cell-regulated mesenchymal factors IGFBP2 and IGFBP3. Our results demonstrate that endothelial cells promote expansion of Kit$^+$ progenitor cells and suppress premature ductal differentiation in early developing embryonic submandibular salivary gland buds.

KEY WORDS: Salivary gland development, Epithelial patterning, Endothelial cells, Ductal differentiation, Progenitor cell, Endothelial cell, Mouse

INTRODUCTION

Organogenesis requires the precise regulation of progenitor cell populations, and how these processes are controlled is currently of great interest. Heterotypic cell interactions are required for organogenesis in many organs, including the salivary gland (Kwon and Larsen, 2015; Nelson and Larsen, 2015). Classical tissue recombination experiments between epithelium and mesenchyme and other studies have demonstrated a requirement for mesenchymal cells in epithelial pattern formation during salivary gland branching morphogenesis. (Hoffman et al., 2002; Tucker, 2007; Wei et al., 2007; Wells et al., 2013; Kera et al., 2014). Additional studies have indicated that Kit$^+$ (Lombaert et al., 2008, 2013; Patel et al., 2014) and cytokeratin 5 (K5; KRT5 – Mouse Genome Informatics)$^+$ (Knox et al., 2013, 2010) epithelial progenitor cells are important for salivary gland development and homeostasis. Kit-expressing progenitor cells were shown to be regulated by fibroblast growth factor produced by the mesenchyme and Kit ligand, which is produced by both the mesenchyme and the epithelium (Lombaert et al., 2013). Developing innervation was shown to regulate the K5$^+$ epithelial progenitor cells (Knox et al., 2010; Nedvetsky et al., 2014; Mattingly et al., 2015), which reciprocally influenced development of the emerging innervation. Involvement of the developing vasculature in salivary gland epithelial development, however, has not been reported.

The circulatory system is connected to every organ and is required for sustaining the viability and function of every adult organ. Studies in several organs, including liver and pancreas, demonstrate a non-nutritional requirement for endothelial cells within the vasculature in early organ patterning prior to the establishment of a functional vascular network (Matsumoto et al., 2001; Lammert et al., 2001; Lazarus et al., 2011; Cleaver and Dor, 2012; Schlieve et al., 2016). Endothelial precursor cells are now acknowledged to produce angiocrine factors, which are paracrine- and juxtacrine-acting factors that control early organ patterning. Multiple angiocrine factors are produced by endothelial cells in every organ, and the profile of angiocrine factors is known to be organ specific (Rafii et al., 2016; Azizoglu and Cleaver, 2016). Angiocrine factors are known to regulate epithelial cell behaviors such as survival and proliferation, polarity, and differentiation (Ingthorsson et al., 2010; Hagiwara et al., 2015; Jaramillo et al., 2015; Kao et al., 2015). Recent evidence demonstrates that vascular endothelial cell-mediated signaling regulates stem/progenitor cell renewal and differentiation during organ development, homeostasis and repair/regeneration (Rafii et al., 2016).

As little is known regarding the relationship between endothelial and epithelial cells during salivary gland development, we hypothesized that endothelial cells have a non-nutritional function in early salivary gland epithelial patterning. To address this hypothesis, we used mouse submandibular salivary gland (SMG) organ explants, which recapitulate the morphogenesis and differentiation of the developing salivary gland *in vivo* (Yamada and Cukierman, 2007; Larsen et al., 2017). With explant culture, it is possible to manipulate the vasculature, without the complications of doing so *in vivo*, in a perfusion-independent manner. We previously identified a number of genes that are expressed in endothelial cells during early SMG branching morphogenesis (Larsen et al., 2017), including vascular endothelial growth factor receptor 2 (VEGFR2), which is also known as fetal liver kinase-1 (Flk-1), kinase insert domain receptor (KDR) and cluster of differentiation 309 (CD309). VEGFR2 is a primary mediator of vascular development and angiogenesis that regulates endothelial cell survival, cell proliferation, and migration (Chavakis and Dimmeler, 2002; Schmidt et al., 2007; Marcelo et al., 2013). We found that pharmacological inhibition and siRNA-mediated genetic manipulation of VEGFR2 signaling in SMG explants

[1]Department of Biological Sciences, University at Albany, State University of New York, 1400 Washington Avenue, Albany, NY 12222, USA. [2]Graduate Program in Molecular, Cellular, Developmental, and Neural Biology, University at Albany, State University of New York, 1400 Washington Avenue, Albany, NY 12222, USA.
*Present address: Cardiovascular Biology Research Program, Oklahoma Medical Research Foundation, 825 North East 13th Street, Oklahoma City, OK 73104, USA.
‡Present address: Regeneron Pharmaceuticals Inc., 81 Columbia Turnpike, Rensselaer, NY 12144, USA.

§Author for correspondence (mlarsen@albany.edu)

M.L., 0000-0002-5026-2012

Received 20 July 2016; Accepted 10 November 2016

Development (2017) 144, 211-220 doi:10.1242/dev.142497

altered epithelial patterning by reducing the number of immature endbuds.

To test the requirement for endothelial cells specifically in salivary epithelial patterning, we developed a novel SMG cell fractionation/reconstitution assay. Using immuno-depletion of the endothelial cells from the mesenchyme of reconstituted glands, we confirmed a requirement for endothelial cells in epithelial patterning. Interestingly, both assays showed a reduction in the Kit progenitor cell population accompanied by increased K19 and K7 in the endbuds with disruption of endothelial cell signaling, and supplementation with exogenous endothelial cells reversed this trend in the SMG cell fractionation/reconstitution assay. To identify endothelial-produced factors that regulate epithelial progenitor cells, we screened conditioned media produced by endothelial cell-depleted and endothelial cell-supplemented mesenchyme. Identified in the screen were secreted factors, including insulin-like growth factor binding protein 2 and 3 (IGFBP2 and IGFBP3), which contributed to the partial restoration of endothelial cell-depleted and VEGFR2-inhibited epithelial organ patterning. We here provide the first evidence of endothelial cell-mediated regulation of epithelial patterning in the developing salivary gland.

RESULTS

Vascular network development is coordinated with branching of the salivary gland epithelium

To determine how patterning of the vasculature relates to patterning of the developing mouse submandibular salivary gland epithelium, we examined the cluster of differentiation 31 (CD31; PECAM1 – Mouse Genome Informatics)$^{+}$ vasculature in embryonic day (E) 11.5-E13.5 submandibular salivary glands (SMGs). SMGs were removed from mouse embryos, fixed, and immediately prepared for immunocytochemistry (ICC) (Fig. 1). Between E11.5 and E12.5, a discontinuous vascular network was evident that included CD31^{+} cell islands and discontinuous vessels within the mesenchyme surrounding the primary epithelial bud (Fig. 1A, B). By E13, fewer endothelial islands were evident with increased CD31^{+} cells present in elongated vascular networks that were distinct from Tubb3^{+} innervation. At E13-E13.5, clefts separate the primary epithelial bud into three to five endbuds concomitant with development of a continuous vessel network. CD31^{+} and VEGFR2^{+} vasculature was frequently detected inside clefts, which are indentations in the basement membrane that subdivide the buds and subsequently define the boundary between the terminal proacinar structures and the emerging secondary ducts (Fig. 1B, C). The schematic in Fig. 1D summarizes the co-development of the vasculature with the epithelium in the early developing SMG.

VEGFR2 signaling and vasculature development promote epithelial patterning in SMG organ explants to favor endbud over duct formation

We previously identified endothelial genes enriched in the clefts of developing salivary glands through data mining of a publicly available salivary gland gene expression database (Larsen et al., 2017). Because one of the cleft-enriched endothelial genes, VEGFR2, is expressed in CD31^{+} endothelial cells (Fig. 1C), and VEGFR2 influences epithelial development in other organs (Matsumoto et al., 2001; Lammert et al., 2001; Lazarus et al., 2011; Magenheim et al., 2011), we manipulated VEGFR2 in salivary gland organ explant cultures. The use of organ explants is ideal for examining the influence of endothelial cell signaling on epithelial pattern formation in a perfusion-independent manner as the explants lack perfusion but recapitulate organ morphogenesis and

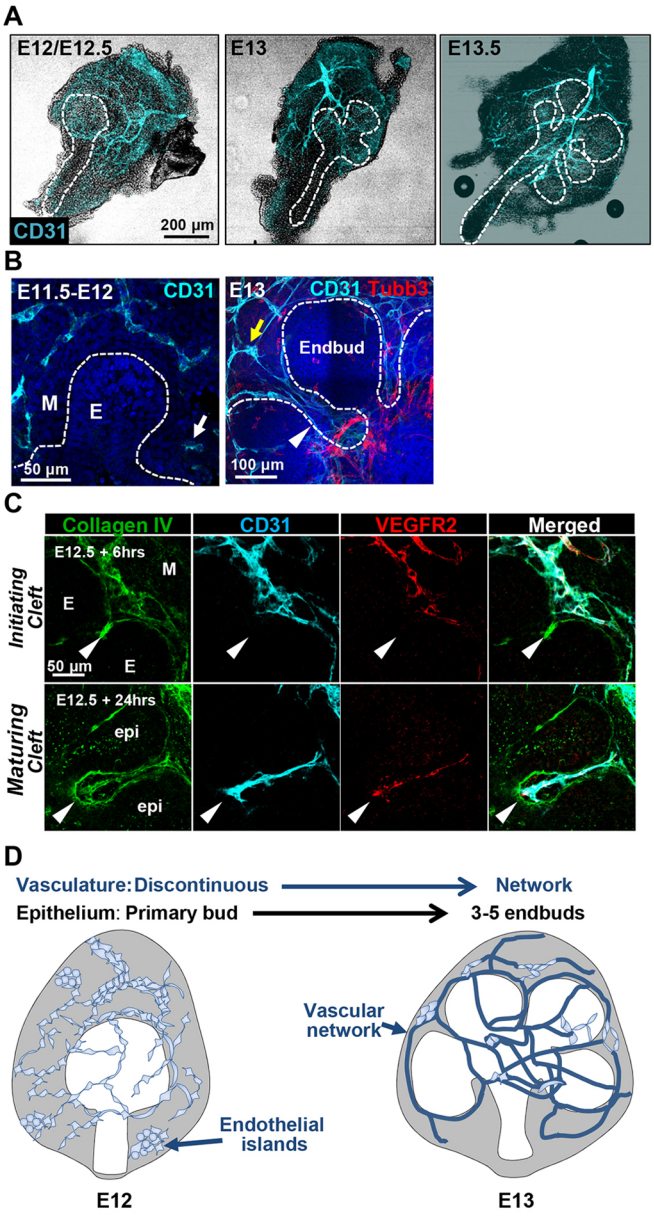

Fig. 1. Co-development of epithelium and vasculature in early developing submandibular gland. (A) Mouse embryonic salivary glands were excised and subjected to ICC and confocal imaging to detect CD31^{+} (cyan) endothelial cells, shown superimposed on a brightfield image. (B) Single confocal images of the glands without brightfield are shown at higher magnification. A CD31^{+} semi-discontinuous vasculature with some isolated endothelial islands (white arrow) was observed in E11.5-E12.5 mesenchyme (M) that was largely isolated from the emerging epithelial bud (E). In E13-E13.5 glands, a largely continuous vessel network (yellow arrow) was observed that progressively surrounds the epithelium and is distinct from the developing nerves (Tubb3^{+}, red). Note that the CD31^{+} vessels penetrate into the maturing epithelial clefts at E13 (white arrowhead). (C) CD31^{+} vessels persist in E12.5 glands cultured *ex vivo* (shown here after 6 h and after 24 h). CD31^{+} endothelial cells also express VEGFR2 (red) and collagen IV (green). Because collagen IV is incorporated into the basement membrane of both the endothelial cells and the epithelial cells, it defines the boundary between the epithelium and mesenchyme. CD31^{+}/VEGFR2^{+}/collagen IV^{+} endothelial cells are found adjacent to the initiating epithelial clefts at E12+6 h growth (arrowheads in upper panels) and ingress into maturing clefts after 24 h of culture (arrowheads in lower panels). (D) Schematic summarizing co-development of the primary epithelial bud with vasculature in the early submandibular gland. Endothelial cells comprising discontinuous vasculature are found in mesenchyme at E12/E12.5. Developing vessels subsequently undergo elongation and maturation concomitant with branching of the primary epithelial bud.

Development (2017) 144, 211-220 doi:10.1242/dev.142497

differentiation *in vivo*. Both pharmacological inhibition with ZM 323881, a selective inhibitor of VEGFR2 tyrosine kinase activity (Whittles et al., 2002), and VEGFR2 siRNA knockdown reduced vasculature development relative to negative controls (Fig. 2A). ICC for cleaved caspase 3 (CC3), an executioner caspase that is activated by cleavage by both extrinsic and intrinsic apoptosis pathways (Salvesen and Dixit, 1997), demonstrated a correlation of CC3 with $CD31^+$ cells, consistent with a loss of endothelial cells due to apoptosis with VEGFR2 inhibition (Fig. S1). Interestingly, VEGFR2 inhibition with ZM 323881 or with SU 5416, a chemically distinct VEGFR2-specific pharmacological inhibitor (Fong et al., 1999), also significantly reduced epithelial branching morphogenesis and altered epithelial patterning in the explants relative to vehicle control (Fig. 2A,B). Similar responses were obtained with VEGFR2 inhibition in cultures of SMGs from E12-E13.5 embryos (Fig. S1). Quantitative evaluation of epithelial morphology in the explants cultured for 48 h indicated that there was reduced branching morphogenesis, as demonstrated by a reduction in total number of endbuds (Fig. 2C), and an increase in the average endbud size (Fig. 2E) with VEGFR2 inhibition. Interestingly, there was an increase in the ratio of ductal area relative to bud area (Fig. 2D), and the widths of the main and secondary ducts were increased upon VEGFR2 inhibition (Fig. 2F,G). Together, these data indicate that VEGFR2 signaling in developing vasculature influences epithelial patterning by promoting branching morphogenesis to favor endbud formation over duct formation.

$CD31^+$ cell-dependent vasculature promotes epithelial patterning by promoting branching morphogenesis in a SMG cell fractionation/reconstitution assay

To investigate further whether $CD31^+$ endothelial cells can influence SMG epithelial patterning, we developed a novel *ex vivo* SMG cell fractionation/reconstitution assay (Fig. 3A). We first microdissected SMG epithelium and mesenchyme and then enzymatically dissociated SMG mesenchyme cells. We then used magnetic-activated cell sorting (MACS)-based immunodepletion to remove $CD31^+$ endothelial cells from the mesenchyme. Unfractionated total mesenchyme cells, mesenchyme immunodepleted of $CD31^+$ endothelial cells, or mesenchyme immunodepleted of $CD31^+$ endothelial cells and supplemented with exogenous $CD31^+$ endothelial cells were then recombined with intact SMG epithelial rudiments. The gland is reconstituted over

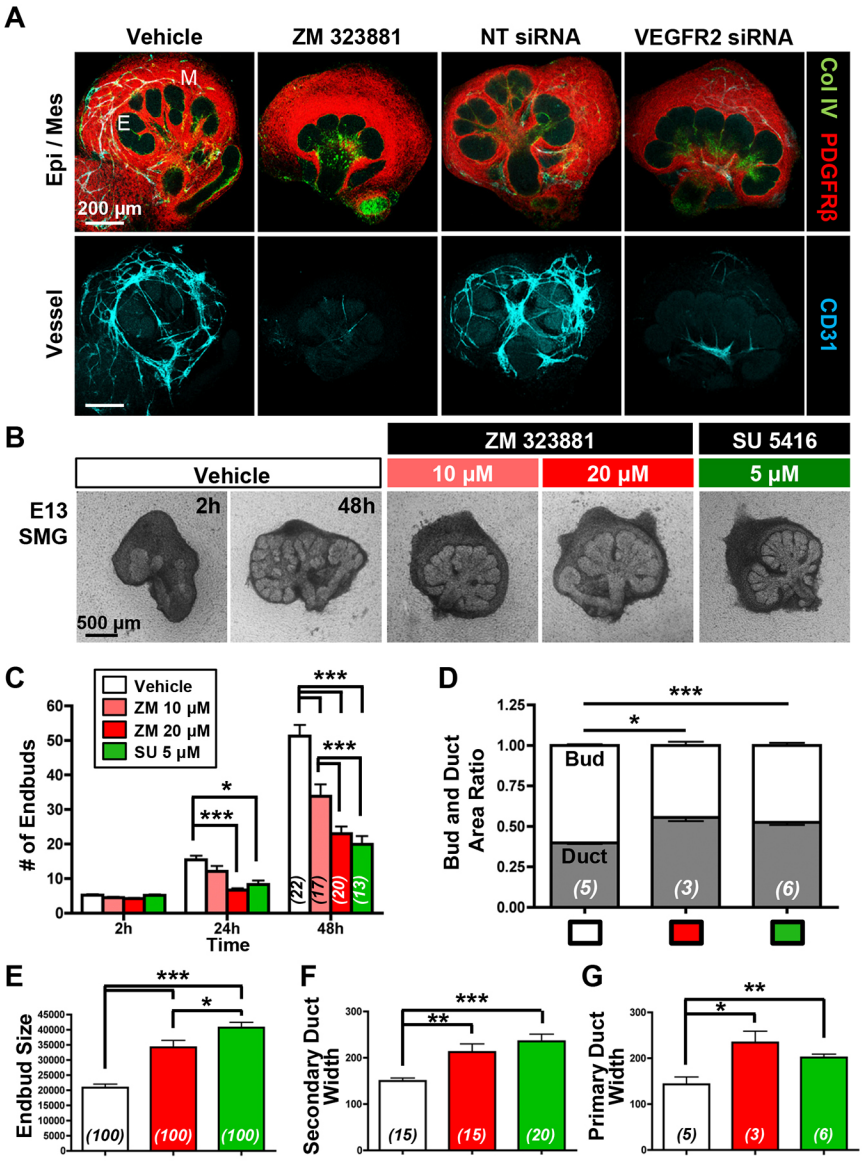

Fig. 2. VEGFR2 signaling and vasculature development promote epithelial patterning in SMG organ culture. (A) Both pharmacological VEGFR2 inhibition (ZM 323881, 20 µM) and VEGFR2 siRNA (400 nM)-mediated knockdown inhibited vascular formation in E12.5 SMG organ explants cultured for 48 h, with reduced $CD31^+$ (cyan) vasculature relative to negative controls, vehicle (DMSO) and non-targeting (NT) siRNA treatment. ICC and confocal microscopy were performed to outline the epithelial basement membrane (Col IV, green), mesenchyme (PDGFRβ, red) and vasculature (Col IV, green; CD31, cyan). Note that the epithelium appears to be less branched upon VEGFR2 inhibition or knockdown. E, epithelial bud; M, mesenchyme. (B) E13 glands were cultured as organ explants in the presence of two distinct VEGFR2 inhibitors (ZM 323881 and SU 5416) for 48 h at the indicated doses, again demonstrating disrupted epithelial organ patterning. (C-G) Brightfield images from multiple glands (*n* indicated on bars) were used to quantify epithelial structures. (C) Endbud numbers in VEGFR2-inhibitor treated glands were significantly reduced in *ex vivo* culture for 24 h and 48 h (*n*=total number of glands from four experiments). (D) The bud/duct ratio of treated glands, compared with vehicle control. Buds were reduced but ducts were enlarged (*n*=number of glands). In inhibitor-treated glands, individual bud size (E) was enlarged (*n*=total number of endbuds from five experiments) and the widths of secondary duct and primary duct (F,G) were widened, respectively (*n*=total number of ducts from five experiments). Data are mean±s.e.m. Two-way ANOVA (C) and Student's *t*-test (one-tailed) (D-G) were performed for statistical analysis (**P*<0.05, ***P*<0.01, ****P*<0.001).

Development (2017) 144, 211-220 doi:10.1242/dev.142497

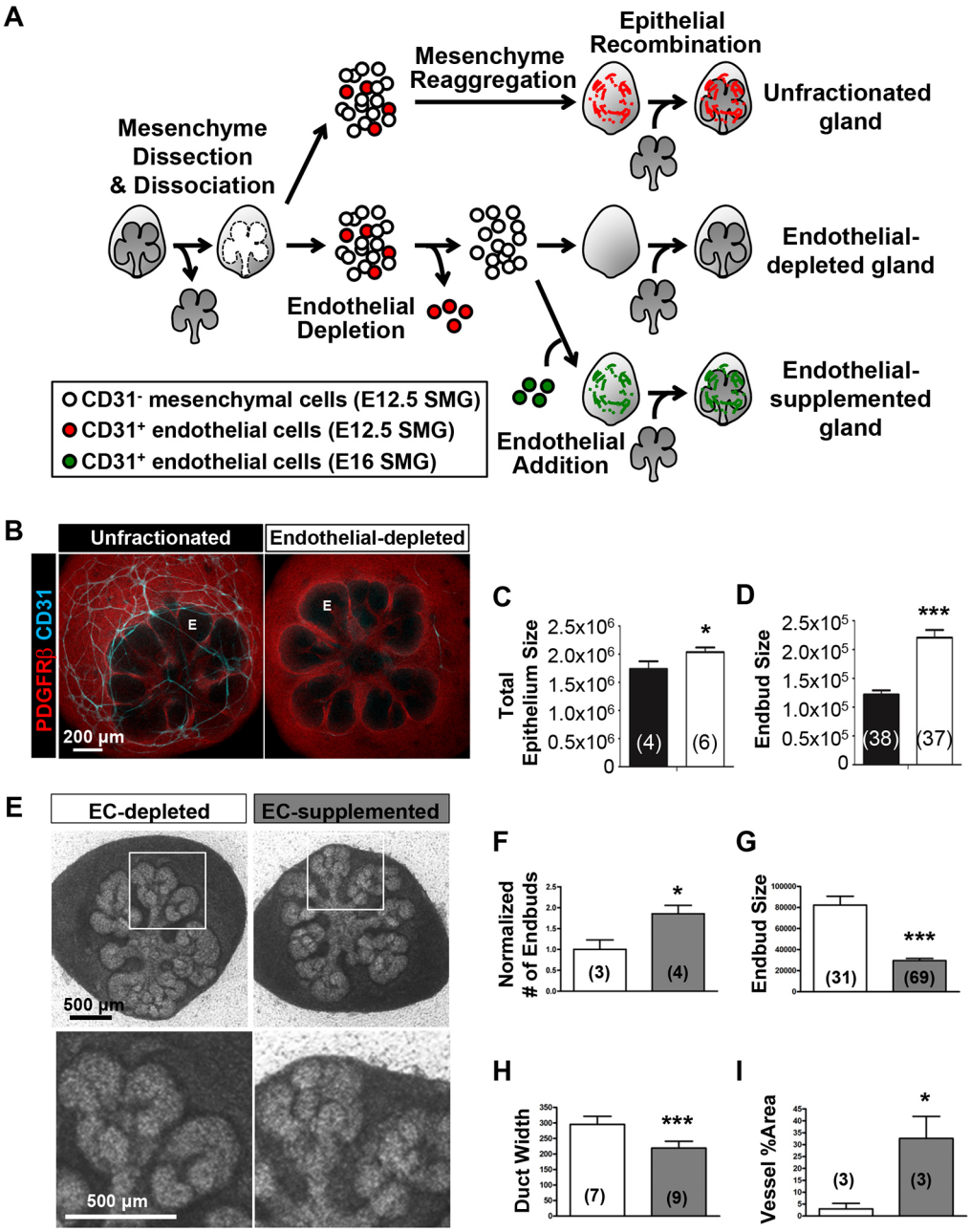

Fig. 3. CD31 cell-dependent vasculature development promotes epithelial patterning in an SMG cell fractionation/reconstitution assay. (A) SMG cell fractionation/reconstitution assay schematic. Unfractionated SMG mesenchyme amenable to cell immunodepletion was generated by microdissection of the mesenchyme from the epithelium followed by enzymatic dissociation of the mesenchyme to single cells and re-aggregation of the isolated mesenchymal cell population. Re-aggregated mesenchyme was then reconstituted with an intact microdissected E13 epithelial rudiment. For endothelial cell depletion, $CD31^+$ endothelial cells were immunodepleted from fully dissociated mesenchyme cells using MACS with CD31 microbeads prior to re-aggregation of the dissociated mesenchyme and reconstitution with an intact epithelium. For endothelial cell supplementation, endothelial-depleted mesenchymal cells were mixed with MACS-isolated endothelial cells prior to re-aggregation of the mesenchyme and reconstitution with an intact epithelium. The reconstituted glands were cultured *ex vivo* for 48 h post-reconstitution. (B) Confocal images (maximum projection images) consistently showed a change in the epithelial patterning (no marker, black) with a mesenchymal marker (PDGFRβ in red) defining the mesenchymal shape. $CD31^+$ vasculature (cyan) was present in unfractionated, but not in endothelial-depleted mesenchyme. E, endbud. (C,D) Epithelial area (C) (*n*=number of reconstituted glands) and endbud size (D) (*n*=number of endbuds from reconstituted glands shown in C) were enlarged in the absence of $CD31^+$ endothelial cells. Black and white bars indicate unfractionated and endothelial-depleted glands, respectively. (E) Supplementation with E16 SMG-derived endothelial cells was performed with endothelial-depleted mesenchyme and epithelial recombination. Reconstituted glands were cultured for 48 h. Boxed areas are enlarged below. (F-H) Endothelial supplementation promoted epithelial branching (F) (*n*=number of reconstituted glands), smaller bud size (G) (*n*=number of endbuds in two reconstituted glands) and thinner ducts (H) (*n*=number of ducts in two reconstituted glands). (I) Increased vessel area was confirmed by CD31 staining in ICCs (*n*=number of reconstituted glands). In F-I, white and gray bars indicate endothelial-depleted (EC-depleted in E) and endothelial-supplemented (EC-supplemented in E), respectively. Data are mean±s.e.m. Student's *t*- test (one-tailed) was performed for statistical analysis (**P*<0.05 ****P*<0.001).

Development (2017) 144, 211-220 doi:10.1242/dev.142497

48 h of culture, and the vasculature reassembles in conditions where CD31$^+$ endothelial cells are included.

To assess the role of endothelial cells in epithelial patterning in the SMG cell fractionation/reconstitution assay, we compared the ability of unfractionated mesenchyme with that of CD31$^+$ endothelial cell-depleted gland mesenchyme to support epithelial branching morphogenesis. ICC confirmed that CD31$^+$ vasculature was absent from CD31$^+$ cell-depleted, reconstituted glands (Fig. 3B). Depletion of endothelial cells and loss of vasculature development lead to significant changes in epithelial morphology 48 h post-reconstitution, with larger endbuds and a considerable increase in the separation of the endbuds relative to unfractionated glands (Fig. 3B). The differences in epithelial morphology between the two conditions were quantified. In endothelial cell-depleted glands, epithelial area (Fig. 3C) and endbud size (Fig. 3D) were increased. To determine whether addition of endothelial cells back into the culture could rescue normal epithelial pattern formation in CD31$^+$ cell-depleted glands, endothelial cell supplementation was performed. Indeed, epithelial branching was promoted by endothelial supplementation (Fig. 3E). Quantitative analysis showed that supplementation promoted more endbuds (Fig. 3F), smaller endbuds (Fig. 3G) and thinner ducts (Fig. 3H). ICC to detect CD31 confirmed partial re-vascularization in the reconstituted glands (Fig. 3I). Together, these data indicate that endothelial cells and vascular development promote branching morphogenesis and normal epithelial patterning during early SMG development and corroborate data obtained using VEGFR2 inhibition/knockdown.

VEGFR signaling and vasculature of SMGs regulate epithelial progenitor cell differentiation

Because depletion of CD31$^+$ endothelial cells impacted the size of developing ducts and the number of endbuds, we wondered whether endothelial cells impact the differentiation of salivary gland epithelial cells within the endbuds. We examined the productal marker K19 together with Kit, a tyrosine kinase expressed by proacinar cells in developing salivary glands (Nelson et al., 2013; Lombaert et al., 2013; Matsumoto et al., 2016). In whole organ explant cultures, VEGFR signaling and vasculature development were manipulated using the pharmacological VEGFR2 inhibitors ZM 323881 and SU 5416. In vehicle-treated E12.5 explants, Kit$^+$ cells and K19$^+$ cells were present in endbuds and ducts, respectively (Fig. 4A). In both ZM 323881- and SU 5416-treated glands, the epithelial pattern was perturbed with apparent longer, wider K19$^+$ developing ducts and expansion of the K19$^+$ productal cells farther from the main duct into the developing buds than in vehicle control glands (Fig. 4A). Quantitative analyses confirmed that gland area positive for Kit decreased whereas the gland area positive for K19 increased in treated glands relative to vehicle-treated controls (Fig. 4B). Analysis of gland areas positive for Kit and K19 in the SMG cell fractionation/reconstitution assay corroborated the inhibitor data in whole gland explant cultures (Fig. 4C). Similarly, increased cells expressing the ductal marker K7 were detected in endbuds both after VEGFR2 inhibition in whole gland explant cultures and after CD31$^+$ endothelial depletion in the SMG cell fractionation/reconstitution assay, which was rescued by CD31$^+$ cell supplementation in the latter assay (Fig. S2). Taken together, these data indicate that VEGFR2-dependent/CD31$^+$ vascular endothelial cells promote the proacinar progenitor cell phenotype in a coordinated manner with branching morphogenesis, and their absence leads to aberrant ductalization of the endbuds.

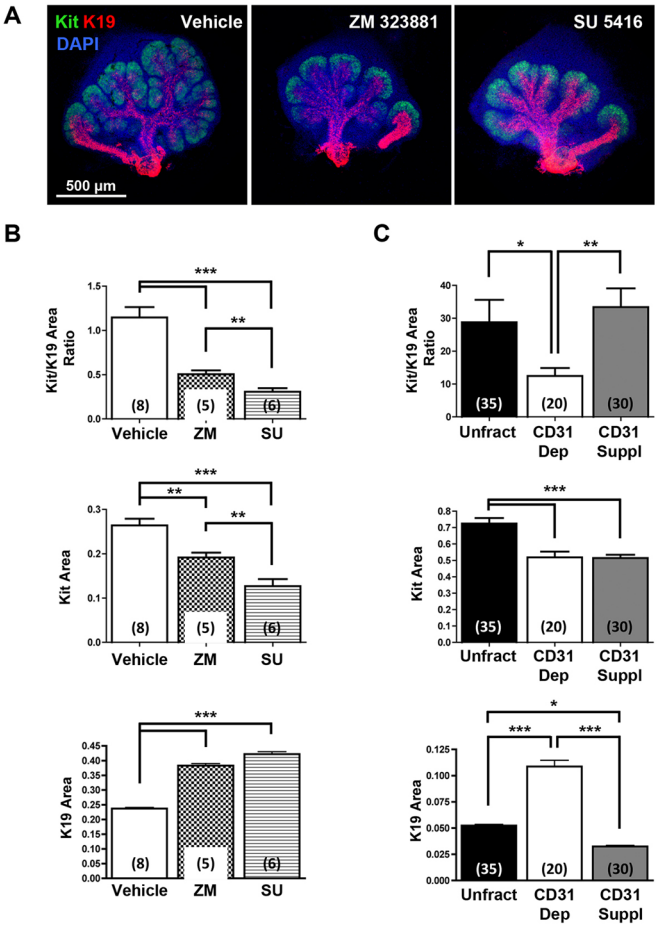

Fig. 4. VEGFR signaling and vasculature development regulate SMG epithelial progenitor cell differentiation. (A) ICC and confocal microscopy show that pharmacological inhibition of VEGFR2 with ZM 323881 (20 µM) or SU 5416 (5 µM) expands the productal K19$^+$ (red) cell population relative to the Kit$^+$ (green) cell population in E12.5 SMGs organ explants grown for 48 h versus control glands. Nuclei were stained with DAPI (blue). (B) Maximum projection intensity images of the glands shown in A were used to quantify areas positive for Kit or K19 within the submandibular epithelium only. Oral epithelium at the base of the main duct was avoided to measure K19 expression area. The Kit$^+$/K19$^+$ ratio was decreased with both inhibitors, and Kit expression area was significantly decreased whereas K19 expression area was significantly increased. (C) In the SMG cell fractionation/reconstitution assay, similar CD31-dependent changes in SMG progenitor cells were also observed, with a marked increase in the K19$^+$ productal cell population. Reconstituted glands were grown for 48 h. Total unfractionated dissociated mesenchyme (Unfract), endothelial depleted (CD31 Dep), endothelial supplementation after endothelial depletion (CD31 Suppl). ICC and confocal microscopy (single section of the middle of endbud) was performed to quantify Kit$^+$ and K19$^+$ expression areas (*n*=number of endbuds). Number of experiments: 7 unfractionated, 4 CD31-depleted and 6 CD31-supplemented. Endothelial cell immunodepletion significantly decreased the Kit$^+$/K19$^+$ ratio, which was partially rescued with endothelial supplementation and re-vascularization. Data are mean±s.e.m. Student's *t*-test was performed for statistical analysis (*P<0.05, **P<0.01, ***P<0.001).

CD31$^+$ endothelial cells influence soluble factors that regulate SMG epithelial patterning and differentiation

Angiocrine factors are juxtacrine- and paracrine-acting factors produced by endothelial cells that influence parenchymal epithelial cell differentiation, homeostasis and regeneration (Rafii et al., 2016). To screen for endothelial cell-dependent soluble factors that might influence the developing SMG epithelium, conditioned media from cultured endothelial cell-depleted mesenchyme and

Development (2017) 144, 211-220 doi:10.1242/dev.142497

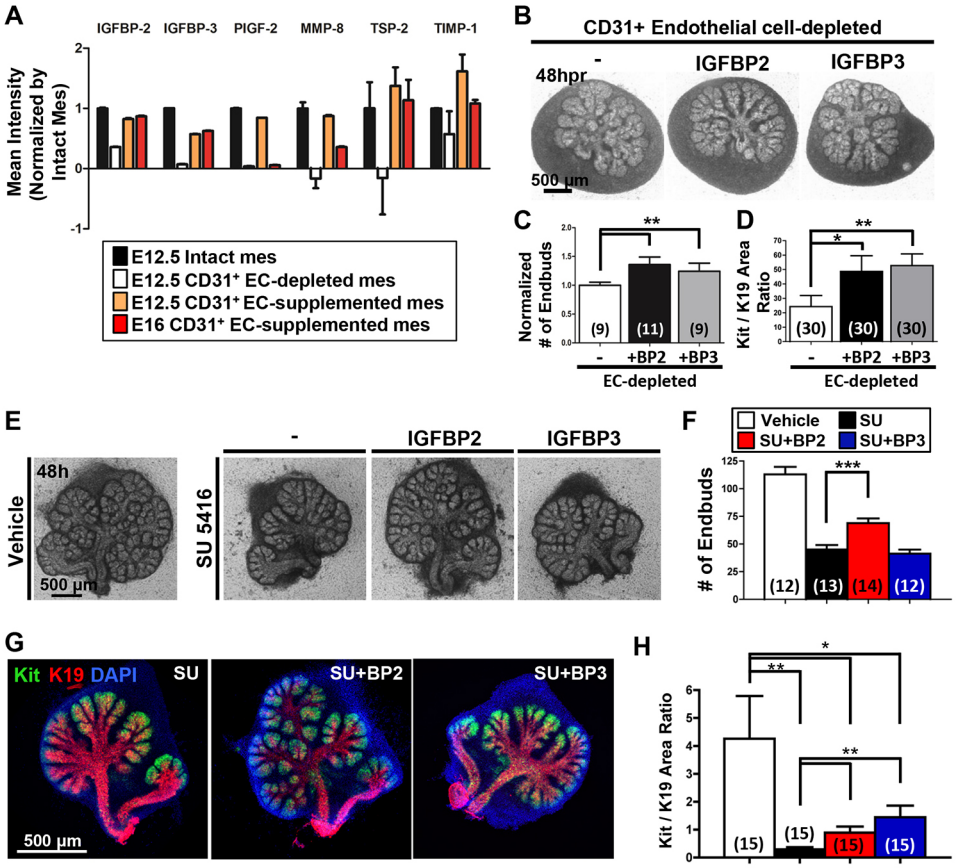

Fig. 5. Vascular endothelial cells influence soluble factors that regulate SMG epithelial patterning and differentiation. (A) Conditioned media collected from intact (black bar) or recombined mesenchyme, including endothelial depletion (white), E12.5 (orange) and E16 (red) CD31$^+$ endothelial supplementation was analyzed with an angiogenesis proteome array. Select soluble factors abundance of which in the conditioned medias changed in response to CD31$^+$ cell condition are shown, normalized to intact mesenchyme. Full normalized data for the array are available in Table S2. (B) Brightfield images of SMG cell glands reconstituted after CD31$^+$ endothelial cell depletion cultured for 48 h without or with addition of recombinant IGFBP2 or IGFBP3 (1 µg/ml). (C,D) Quantitative analyses demonstrate that both IGFBP2 and IGFBP3 supplementation increased epithelial branching (C) (*n*=number of reconstituted glands) and the Kit$^+$/K19$^+$ area ratio (D) (*n*=total number of endbuds from six reconstituted glands). (E) Brightfield images of E13 SMG explants cultured *ex vivo* for 48 h in the absence or presence of 5 µM SU 5416 (SU), either with or without addition of recombinant IGFBP2 (BP2; 2 µg/ml) or IGFBP3 (BP3; 5 µg/ml). (F) Quantitative analysis of VEGFR2-inhibited glands shows disrupted epithelial patterning expressed as endbud numbers (three experiments). (G) ICC and confocal images representative of the partial rescue of Kit (green) relative to K19 (red) expression areas in the IGFBP2- and IGFBP3-supplemented, SU 5416-treated glands. (H) The Kit$^+$/K19$^+$ ratio was partially rescued with exogenous IGFBPs (*n*=total number of endbuds from three experiments). Data are mean±s.e.m. Student's *t*-test was performed for statistical analysis (**P*<0.05, ***P*<0.01, ****P*<0.001).

endothelial supplemented mesenchyme were applied to an antibody-based proteome array containing 53 soluble factors. Intact mesenchyme pieces were used as a positive control. Multiple factors were more abundant in the conditioned media collected from the CD31$^+$ cell-supplemented mesenchyme cell cultures relative to the CD31$^+$ cell-depleted mesenchyme, including IGFBP2, IGFBP3, PIGF-2 (PGF), MMP8, TSP-2 (THBS2 – Mouse Genome Informatics) and TIMP1 (Fig. 5A).

As IGFBP2 and IGFBP3 gave robust signals on the proteome array and have previously been identified as angiocrine factors (Remédio et al., 2012; Minuzzo et al., 2015; Rafii et al., 2016), we tested whether these factors can rescue epithelial patterning upon vasculature disruption using recombinant IGFBP2 or IGFBP3 added to SMG culture assays. In the SMG cell fractionation/reconstitution assay, addition of recombinant IGFBP2 or IGFBP3 promoted both epithelial patterning (Fig. 5B,C) and differentiation (Fig. 5D) relative to CD31$^+$ cell depleted samples. We also tested the effects of recombinant IGFBP2 or IGFBP3 in intact gland explant assays, in which IGFBP2, but not IGFBP3, showed a partial rescue of disrupted epithelial branching in the SU 5416-inhibited glands (Fig. 5E,F). Similar to the SMG cell fractionation/reconstitution assay, ICC of Kit$^+$ and K19$^+$ cells in the endbuds of SU 5416-treated glands revealed that the reduction of the Kit$^+$/K19$^+$ ratio with VEGFR2 inhibition was partially rescued by exogenous IGFBP2 or IGFBP3 (Fig. 5G,H). We performed additional arrays to interrogate the cell type that makes IGFBP2 and IGFBP3. We found that IGFBP2 and IGFBP3 are made primarily by the mesenchyme relative to the epithelium. Interestingly, we noted that both the endothelial cells and the non-endothelial mesenchyme make these proteins, with more robust production by the non-endothelial mesenchyme (Fig. S3). Together, these data indicate that vascular endothelial cells promote epithelial patterning and differentiation at least in part through effects on soluble factors, such as IGFBPs.

DISCUSSION

Signaling from mesenchymal cell subpopulations is required for elaboration of epithelial tissue structure during development. Using an SMG cell fractionation/reconstitution assay that allowed us to deplete CD31$^+$ endothelial cells from the mesenchyme of reconstituted embryonic submandibular salivary glands, we

Development (2017) 144, 211-220 doi:10.1242/dev.142497

demonstrate for the first time that CD31$^+$ endothelial cells influence epithelial patterning during salivary gland development in a perfusion-independent manner. The endothelial cells function through VEGFR2-dependent signaling to moderate ductalization of the buds and support the Kit$^+$ bipotent progenitor cell population. We observed that inhibition of this vasculature-dependent support of progenitor cell expansion caused altered epithelial patterning through reduction of the Kit$^+$ cell population that was accompanied by increased localization of K19$^+$ and K7$^+$ ductal cells in the endbuds of the gland. This would be predicted to prevent normal elaboration of the secretory compartment of the gland with accumulation of elongated and dilated ducts. In fact, similar pathologies are associated with diseases that result in xerostomia, such as Sjögren's syndrome and irradiation damage as a result of treatment of head and neck cancers, suggesting that a continued interaction of the vasculature and the epithelium may be a component of homeostasis or a response to injury in adult glands. Consistent with our findings in development, several studies have suggested that the vasculature is damaged in salivary gland pathologies and that gland regeneration is enhanced by restoration of the vasculature (Cotrim et al., 2007; Zhang et al., 2014; An et al., 2015).

Endothelial cells instruct organ development in other organs, such as liver (Matsumoto et al., 2001), pancreas (Lammert et al., 2001; Cleaver and Dor, 2012) and lung (Lazarus et al., 2011), through perfusion-independent mechanisms prior to the formation of functional vasculature. In the liver, VEGFR2-dependent signaling is required for early hepatocyte morphogenesis and differentiation (Matsumoto et al., 2001) and cell fate specification of the central zone of the liver (Rocha et al., 2015). Similarly, early dorsal pancreas budding and insulin production by β cells requires endothelial cell signaling (Lammert et al., 2001; Yoshitomi and Zaret, 2004). However, endothelial cell signaling can also restrict cell fate. VEGFR2-dependent endothelial cell signaling restricts branching morphogenesis and restricts acinar differentiation later in development of the pancreas (Magenheim et al., 2011) and differentiation in liver (Ramasamy et al., 2015; Rocha et al., 2015). Determining which cells are directly impacted by endothelial-dependent signaling in developing salivary glands and whether cell fate choices are directly regulated by VEGFR2 signaling will require investigation by cell lineage tracking.

Although specific angiocrine factors produced by endothelial cells can regulate cell specification, such as R-spondin 3 in specification in the liver (Rocha et al., 2015), endothelial cell signaling can also activate signaling by other mesenchyme cells to regulate progenitor cells indirectly in the epithelium. For example, endothelial-produced factors are known to recruit and support stromal pericytes, which are important for organogenesis. Additionally, endothelial progenitor cell-produced platelet-derived growth factor (PDGF)-BB was identified in recruitment and sustaining the function of the PDGFRβ$^+$ mesenchymal stem cells (MSCs) after therapeutic engraftment during MSC cell therapy (Lin et al., 2014). Although IGFBP2 is known to be one of many angiocrine factors produced by endothelial cells in an organ-specific manner (Mouhieddine et al., 1996; Besnard et al., 2001; Bridgewater and Matsell, 2003; Huynh et al., 2011; Perri et al., 2014), in the salivary gland, IGFBP2 and IGFBP 3 appear to be produced primarily by CD31$^-$ mesenchyme cells.

Our data are consistent with a model in which endothelial cells stimulate IGFBP2 and IGFBP3 production by neighboring mesenchymal cells, and IGFBP2 and IGFBP3 produced by mesenchymal cells modulate epithelial signaling in developing salivary glands to favor Kit$^+$ cells over K19$^+$ cells in the developing endbuds. IGFBP2 in circulation can stimulate or inhibit the growth-promoting effects of the IGFs (Binkert et al., 1992; Bourner et al., 1992). However, IGFBP2 has an RGD site that can activate integrin signaling independently of IGF receptors (Feng et al., 2015), and modulates the expansion and survival of hematopoietic stem cells (Huynh et al., 2011). Whether IGFBP2 and IGFBP3 function in an IGF-dependent or -independent manner in an *in vivo* context during salivary gland development and how they regulate epithelial progenitor cells remains to be elucidated. Although our data do not delineate a specific mechanism for endothelial cell signaling in controlling SMG cell fate, they are consistent with data from other embryonic organs indicating that the developing vasculature supports expansion of the primitive progenitor populations, which in turn recruits developing vasculature to the emerging epithelium.

A similar premature ductal differentiation was recently reported during early development of the salivary gland that is Wnt dependent (Matsumoto et al., 2016). Similar to our data demonstrating premature ductal formation and expansion of the ductal area of the gland with compromised VEGFR2/CD31$^+$ endothelial cell function, Matsumoto et al. observed that excess Wnt signaling can induce premature ductal formation and expansion of the ductal compartment of the gland. In early SMG development, mesenchymal Wnt signaling antagonized FGF-mediated proacinar cell differentiation to expand the Kit$^+$ distal progenitor cell population. As mesenchymal Wnt signaling declines at E15 concomitant with the onset of cytodifferentiation, they show that the expanded bipotent Kit$^+$ progenitor population then creates the secretory proacinar and emerging secondary duct structures required for development of the mature branched organ. Wnt signaling can also suppress Kit expression at the RNA level through Myb, demonstrating that Wnt activity must be tightly balanced to allow proper progenitor expansion followed by spatially restricted differentiation.

In our studies, the VEGFR2/CD31$^+$ endothelial cell population might promote epithelial patterning and expansion of the Kit$^+$ endbud epithelial progenitor cell population in part by modulating Wnt signaling from the mesenchyme. Loss of VEGFR2/CD31$^+$ endothelial cell function would then be expected to increase canonical Wnt signaling to the epithelium, prevent proacinar differentiation, downregulate Kit expression and accelerate ductal formation. Wnt signaling is regulated by balancing activation of Wnt receptors by ligands at many levels, and several reports indicate that the Wnt family has complex roles in SMG development (Haara et al., 2011; Musselmann et al., 2011; Patel et al., 2011; Knosp et al., 2015; Maimets et al., 2016; Matsumoto et al., 2016). Thus, VEGFR2/CD31$^+$ endothelial cells could act in many ways to modulate mesenchymal Wnt signaling to the epithelium, and might confer this regulation in a spatially restricted manner during branching morphogenesis. Thus, the mesenchyme, including the PDGFRβ$^+$ fibroblasts, vasculature and innervation (Knox et al., 2010), develops in a coordinated manner with the epithelium, and this co-patterning is likely to confer essential spatial restriction to the reciprocal epithelial-mesenchymal signaling pathways that control organ development.

Diverse, reciprocal signaling pathways between the epithelium and mesenchyme are known to orchestrate SMG development, and the mechanisms by which these signals interact and are decoded by the progenitor cell populations to coordinate morphogenesis and differentiation are of great interest. Reciprocal interactions between the developing vasculature and epithelium are likely to be multifactorial, similar to the contribution of innervation to gland development (Knox et al., 2010; Nedvetsky et al., 2014; Knosp

Development (2017) 144, 211-220 doi:10.1242/dev.142497

et al., 2015). The fact that our assays with IGFBP2 and IGFBP3 show modest effects on SMG morphogenesis and differentiation is consistent with the concept that there are likely to be numerous endothelial-produced factors that impact parenchymal development. As addition of excess recombinant proteins cannot recapitulate spatial restriction of signaling factors, additional studies will be needed to confirm a role for these factors in SMG *in vivo* development and elucidate the mechanism by which they control epithelial patterning of differentiation.

Importantly, our SMG cell fractionation/gland reconstitution assay provides a platform for more extensive screens for putative angiocrine factors (soluble or cell-cell mediated) as well as for mechanistic studies that cannot be performed with classical organ recombination experiments using intact mesenchyme. Additionally, the SMG cell fractionation/reconstitution assay enables screening for synthetic or interacting pathways, for example with $CD31^+$ cell depletion/cell supplementation in the presence of inhibitors or genetic knockdown of other pathways known to control gland development. Recent work in lung branching morphogenesis and differentiation revealed that mesenchymal glucocorticoid receptor and STAT3 act in parallel pathways to specify lung alveolar differentiation, such that neither is absolutely required but either pathway can promote epithelial differentiation (Laresgoiti et al., 2016). Our gland reconstitution assay will facilitate future investigation of these types of parallel, or similarly synergistic, activities in epithelial cell fate choices. The assay is also amenable for testing the interaction between mesenchymal cell subsets, such as vascular cells and nerves, which are known to have reciprocal patterning effects in other systems.

Elucidation of the molecular mechanisms through which the vasculature directly instructs epithelial patterning and differentiation, as well pathways through which it affects other mesenchymal cell types to indirectly affect the parenchymal epithelium, will ultimately enable therapeutic manipulations. Similarities and differences in the angiocrine control of organ development and regeneration in diverse organs can be exploited to enhance both general and organ-specific regenerative medicine approaches. Importantly, the angiocrine mechanisms that control organ homeostasis and response to injury are currently being characterized and exploited for therapeutic interventions to improve organ regeneration (Rafii et al., 2016). Ongoing characterization of angiocrine control of salivary glands might similarly improve therapeutic options for restoration of salivary gland function in disease pathologies.

MATERIALS AND METHODS

Ex vivo SMG organ explant culture with pharmacological and siRNA manipulation

Salivary gland dissection and *ex vivo* culture were performed according to previously established methods (Daley et al., 2009) and protocols approved by the University at Albany Institutional Animal Care and Use Committee. Embryos were harvested from timed pregnant CD-1 female mice (Charles River) at the embryonic stages indicated for each figure (with day of plug discovery designated as E0). SMGs were removed from the embryos under a dissecting microscope. The SMGs were placed on a polycarbonate filter with 0.1 µm pores (Nuclepore, GE Healthcare Life Sciences) in a glass-bottomed, single-microwell dish (MatTek) and cultured *ex vivo* in complete DMEM/F12 medium [1:1 DMEM/Ham's F12 lacking Phenol Red (Invitrogen) supplemented with 50 µg/ml transferrin, 150 µg/ml L-ascorbic acid, 100 U/ml penicillin and 100 µg/ml streptomycin].

Pharmacological and siRNA treatments were performed in whole explants. For pharmacological VEGFR2 inhibition, ZM 323881 (10 µM and 20 µM in DMSO; Tocris) (Whittles et al., 2002) and SU 5416 (5 µM in DMSO; Tocris) (Fong et al., 1999) were supplemented during the explant culture. Vehicle-treated controls contained the same volume of DMSO. siRNA genetic manipulation was performed as previously described (Daley et al., 2009). VEGFR2 siRNAs (Silencer Select s68715/s68716, Thermo Fisher Scientific) and negative control non-targeting siRNA (Silencer Select Negative Control #2 siRNA) were transfected using RNAiFECT (Qiagen), both at a final concentration of 400 nM.

For mesenchyme-free, epithelial rudiment cultures, epithelial rudiments were physically separated from mesenchyme following a dispase digestion, as previously described (Sequeira et al., 2013), and were cultured *ex vivo* for 48 h in growth factor-reduced Matrigel (Corning, 356231). FGF7 (200 ng/ml; Peprotech, 100-19) and epidermal growth factor (20 ng/ml; Peprotech, AF-100-15) were additionally supplemented into the complete DMEM/F12 medium.

Primary mesenchyme cell preparation

To prepare unfractionated E12/E13 mesenchyme, dispase digestion of E12/E13 whole SMGs was performed followed by manual separation of the mesenchyme from the epithelium, as previously described (Sequeira et al., 2013). To prepare E12/E13 primary mesenchyme cells, mesenchyme pieces were placed into a MatTek dish, mixed with 200 µl 0.3× collagenase/hyaluronidase (7912, STEMCELL Technologies, Vancouver, Canada), and incubated for 5 min at 37°C. The digested mesenchyme was mixed with 20 µl fetal bovine serum (FBS; Life Technologies), placed in a microcentrifuge tube, and homogenized by trituration 30-40 times to yield single cells.

To prepare primary E16 mesenchyme cells, whole excised E16 SMGs were microdissected with forceps in a 35 mm dish and serially treated with 1× collagenase/hyaluronidase (STEMCELL Technologies) for 10 min and 0.8 U/ml dispase (Life Technologies) for 10-15 min, followed by incubation for 15 min at 37°C. The cell preparation was mixed with 200 µl FBS, placed into a 15 ml conical tube, and homogenized by trituration at least 40 times. To enrich for mesenchymal cells, the epithelial fragments were separated by gravity sedimentation for 5 min. The mesenchyme-enriched gravity supernatant was filtered through a 70 µm pore size cell strainer (Falcon) to enrich for single cells, and washed twice with PBS with 10% FBS/2 mM ethylenediaminetetraacetic acid (EDTA; Sigma-Aldrich) buffer. The enriched primary mesenchymal cells were centrifuged at 450 ***g*** for 5 min and re-suspended in 1× PBS buffer with 10% FBS and 2 mM EDTA.

Depletion of $CD31^+$ cells from mesenchyme and collection of $CD31^+$ cells by magnetic-activated cell sorting (MACS)

For $CD31^+$ endothelial cell depletion from E12.5 primary mesenchyme, MACS with mouse CD31 microbeads (130-097-418, Miltenyi Biotech, Bergisch Gladbach, Germany) was performed according to the manufacturer's protocols. Briefly, enriched primary mesenchyme cells were suspended in 99 µl 1× PBS buffer with 10% FBS and mixed with 1 µl mouse CD31 microbeads, followed by incubation at 4°C for 15 min. After washing with 500 µl PBS buffer with 10% FBS, the microbead-incubated cells were centrifuged at 450 ***g*** for 5 min and resuspended with 200 µl PBS with 10% FBS for immunomagnetic separation. To collect $CD31^-$ mesenchyme, cells were applied to a magnetic column and the flow-through was collected, followed by three washes with 1× PBS with 10% FBS, which were included with the flow-through. The remaining $CD31^+$ cells were collected by centrifugation at 450 ***g*** for 5 min and then resuspended in DMEM:F12 medium.

For isolation of $CD31^+$ endothelial cells from E16 SMG, primary E16 mesenchyme cells were prepared as described above, and negative selection was performed to remove contaminating $EpCAM^+$ epithelial cells. Primary mesenchyme cells were resuspended in 90 µl PBS with 10% FBS/2 mM EDTA buffer (wash buffer), mixed with 10 µl mouse EpCAM microbeads (130-105-958, Miltenyi Biotech), followed by incubation at 4°C for 15 min. After washing with 1 ml wash buffer, the microbead-incubated cells were centrifuged at 450 ***g*** for 5 min and resuspended in 500 µl wash buffer for magnetic removal of the $EpCAM^+$ cells. The resulting mesenchymal cells were collected and centrifuged at 450 ***g*** for 5 min, resuspended in 90 µl wash buffer, mixed with 10 µl mouse CD31 microbeads, and incubated at 4°C for 15 min. Positive selection was performed to collect the $CD31^+$ endothelial cells.

Development (2017) 144, 211-220 doi:10.1242/dev.142497

SMG cell fractionation/reconstitution assay

Dissociated whole unfractionated mesenchyme cells, CD31$^-$ mesenchyme cells, or CD31$^-$ mesenchyme cells supplemented with purified CD31$^+$ endothelial cells were cultured overnight. For overnight cultures, the mesenchyme cell fractions were collected and centrifuged at 450 ***g*** for 5 min. Cells were then suspended in 50 µl fresh DMEM:F12 medium containing only antibiotics (100 U/ml penicillin and 100 µg/ml streptomycin) and placed into a V-bottom 96-well plate to encourage mesenchymal tissue reaggregation overnight at 37°C. The contracted mesenchymal tissue was placed on a Nuclepore filter in a MatTek dish with a fresh intact E13 SMG epithelium placed on top of the aggregated mesenchyme to reconstitute the gland. The reconstituted glands were grown with complete DMEM/F12 organ explant medium for 48 h. Each reconstituted gland was considered to be a single experiment.

Immunocytochemistry and confocal microscopy

Immunocytochemistry (ICC) was performed as previously described (Daley et al., 2009; Peters et al., 2015). Briefly, SMG organ explants or SMG cell fractionation/reconstitutions glands were fixed with 4% paraformaldehyde (w/v) (Electron Microscopy Sciences) containing 5% sucrose (w/v) for 20 min at room temperature (RT) and permeablized with 0.1% Triton X-100 (Sigma-Aldrich) or fixed/permeablized in 100% cold MeOH at −20°C. Blocking was performed with 20% donkey serum in 1× PBS with 0.5% Tween-20 for 1 h at RT. Primary and secondary antibodies were diluted in 1× PBS with 0.5% Tween-20 and incubated overnight at 4°C or for 1.5 h at room temperature, and then washed three times in PBS with 0.5% Tween-20. Antibodies and the dilutions used in this study are shown in Table S1. DAPI (Life Technologies) was used for nuclear staining. The tissues were mounted with Fluoro-Gel (Electron Microscopy Sciences) and imaged with a Zeiss 510 or 710 confocal microscope (Carl Zeiss).

Angiogenesis proteomic array

For analysis of soluble factors, microdissected mesenchyme pieces, endothelial-depleted mesenchyme or endothelial-supplemented mesenchyme were cultured for 48 h to collect conditioned media. Conditioned media was applied to a mouse angiogenesis proteome array (Proteome Profiler Mouse Angiogenesis Antibody Array, #ARY015, R&D systems) and samples were processed according to the manufacturer's protocol. For analysis of factor production, cell lysates were prepared as previously described (Larsen et al., 2003). Briefly, gland tissue or cells were collected in a microfuge tube and solubilized with completed RIPA buffer (Thermo Fisher Scientific) containing complete mini, EDTA-free protease inhibitor cocktail (Roche), followed by sonication and centrifugation at 4°C to collect the soluble fraction. The resulting cell lysates of fresh uncultured microdissected E12.5 epithelium, mesenchyme, E12/E13 CD31$^-$ depleted mesenchyme, or immunopurified CD31$^+$ endothelial cells were applied to the angiogenesis proteome array. Image processing to measure spot intensities from films was performed using ImageJ software (National Institute of Health). Duplicate spots within each membrane were used to calculate average intensities. The normalized spot intensity was calculated as (individual spot intensity−negative spot intensity)/positive spot intensity. Additional normalization procedures are explained in each figure legend when relevant.

Image data analysis for epithelial patterning and differentiation

To evaluate epithelial structure, measurements of epithelium size, endbud/duct area, endbud size, or duct width/length were collected from brightfield images of SMG organ explants or SMG cell fractionation/reconstitution glands. Area and size were measured as the pixel area value of manually designated areas, and width and length were collected from pixel length value using ImageJ. Percentages of Kit$^+$ and K19$^+$areas were measured from ICC confocal images. First, total epithelium or individual endbuds were manually designated using the polygon selection tool, as indicated in figure legends. Individual Kit$^+$ and K19$^+$ areas were calculated and normalized to total designated area; each marker-positive pixel area value (measured using a threshold option) was divided by the total pixel area of the designated area. To analyze apoptotic endothelial cells (double-positive CD31$^+$ and cleaved caspase 3$^+$ cells), CD31$^+$ areas were manually designated and the cleaved caspase 3$^+$ area was measured using a threshold tool. Vessel area (the area of the segmented CD31$^+$ vessel area/total area) was measured using AngioTool (Zudaire et al., 2011) (https://ccrod.cancer.gov/confluence/display/ROB2/Home). Vessel intensity was evaluated by CD31 staining of confocal images using ImageJ. Graphs were prepared using Prism 5 (GraphPad). Statistics were calculated as described in each figure using Prism 5 and Microsoft Excel.

Acknowledgements

The authors thank Drs Guohao Dai, Paolo Forni and Prashanth Rangan for helpful comments.

Competing interests

The authors declare no competing or financial interests.

Author contributions

H.R.K., M.L., and D.A.N. conceived the experiments. H.R.K., K.A.D., and J.M.M. performed the experiments. H.R.K., M.L., and D.A.N. interpreted the data. H.R.K., M.L., and D.A.N. wrote and revised the manuscript.

Funding

This work was supported by the National Institutes of Health (RO1 DE022467 to M.L., C06 RR015464) and the University at Albany (SUNY). Deposited in PMC for release after 12 months.

Supplementary information

Supplementary information available online at
http://dev.biologists.org/lookup/doi/10.1242/dev.142497.supplemental

References

An, H. Y., Shin, H. S., Choi, J. S., Kim, H. J., Lim, J. Y. and Kim, Y. M. (2015). Adipose mesenchymal stem cell secretome modulated in hypoxia for remodeling of radiation-induced salivary gland damage. *PLoS ONE* **10**, e0141862.

Azizoglu, D. B. and Cleaver, O. (2016). Blood vessel crosstalk during organogenesis-focus on pancreas and endothelial cells. *Wiley Interdiscip. Rev. Dev. Biol.* **5**, 598-617.

Besnard, V., Corroyer, S., Trugnan, G., Chadelat, K., Nabeyrat, E., Cazals, V. and Clement, A. (2001). Distinct patterns of insulin-like growth factor binding protein (IGFBP)-2 and IGFBP-3 expression in oxidant exposed lung epithelial cells. *Biochim. Biophys. Acta* **1538**, 47-58.

Binkert, C., Margot, J. B., Landwehr, J., Heinrich, G. and Schwander, J. (1992). Structure of the human insulin-like growth factor binding protein-2 gene. *Mol. Endocrinol.* **6**, 826-836.

Bourner, M. J., Busby, W. H., Siegel, N. R., Krivi, G. G., McCusker, R. H. and Clemmons, D. R. (1992). Cloning and sequence determination of bovine insulin-like growth factor binding protein-2 (IGFBP-2) - comparison of its structural and functional properties with IGFBP-1. *J. Cell. Biochem.* **48**, 215-226.

Bridgewater, D. J. and Matsell, D. G. (2003). Insulin-like growth factor binding protein-2 modulates podocyte mitogenesis. *Pediatr. Nephrol.* **18**, 1109-1115.

Chavakis, E. and Dimmeler, S. (2002). Regulation of endothelial cell survival and apoptosis during angiogenesis. *Arterioscler. Thromb. Vasc. Biol.* **22**, 887-893.

Cleaver, O. and Dor, Y. (2012). Vascular instruction of pancreas development. *Development* **139**, 2833-2843.

Cotrim, A. P., Sowers, A., Mitchell, J. B. and Baum, B. J. (2007). Prevention of irradiation-induced salivary hypofunction by microvessel protection in mouse salivary glands. *Mol. Ther.* **15**, 2101-2106.

Daley, W. P., Gulfo, K. M., Sequeira, S. J. and Larsen, M. (2009). Identification of a mechanochemical checkpoint and negative feedback loop regulating branching morphogenesis. *Dev. Biol.* **336**, 169-182.

Feng, N., Zhang, Z., Wang, Z., Zheng, H., Qu, F., He, X. and Wang, C. (2015). Insulin-like growth factor binding protein-2 promotes adhesion of endothelial progenitor cells to endothelial cells via integrin alpha 5 beta 1. *J. Mol. Neurosci.* **57**, 426-434.

Fong, T. A., Shawver, L. K., Sun, L., Tang, C., App, H., Powell, T. J., Kim, Y. H., Schreck, R., Wang, X., Risau, W. et al. (1999). SU5416 is a potent and selective inhibitor of the vascular endothelial growth factor receptor (Flk-1/KDR) that inhibits tyrosine kinase catalysis, tumor vascularization, and growth of multiple tumor types. *Cancer Res.* **59**, 99-106.

Haara, O., Fujimori, S., Schmidt-Ullrich, R., Hartmann, C., Thesleff, I. and Mikkola, M. L. (2011). Ectodysplasin and Wnt pathways are required for salivary gland branching morphogenesis. *Development* **138**, 2681-2691.

Hagiwara, M., Peng, F. and Ho, C.-M. (2015). In vitro reconstruction of branched tubular structures from lung epithelial cells in high cell concentration gradient environment. *Sci. Rep.* **5**, 8054.

Development (2017) 144, 211-220 doi:10.1242/dev.142497

Hoffman, M. P., Kidder, B. L., Steinberg, Z. L., Lakhani, S., HO, S., Kleinman, H. K. and Larsen, M. (2002). Gene expression profiles of mouse submandibular gland development: FGFR1 regulates branching morphogenesis in vitro through BMP- and FGF-dependent mechanisms. *Development* **129**, 5767-5778.

Huynh, H., Zheng, J., Umikawa, M., Zhang, C., Silvany, R., Iizuka, S., Holzenberger, M., Zhang, W. and Zhang, C. C. (2011). IGF binding protein 2 supports the survival and cycling of hematopoietic stem cells. *Blood* **118**, 3236-3243.

Ingthorsson, S., Sigurdsson, V., Fridriksdottir, A. J. R., Jonasson, J. G., Kjartansson, J., Magnusson, M. K. and Gudjonsson, T. (2010). Endothelial cells stimulate growth of normal and cancerous breast epithelial cells in 3D culture. *BMC Res. Notes* **3**, 184.

Jaramillo, M., Mathew, S., Mamiya, H., Goh, S. K. and Banerjee, I. (2015). Endothelial cells mediate islet-specific maturation of human embryonic stem cell-derived pancreatic progenitor cells. *Tissue Eng. Part A* **21**, 14-25.

Kao, D.-I., Lacko, L. A., Ding, B.-S., Huang, C., Phung, K., Gu, G., Rafii, S., Stuhlmann, H. and Chen, S. (2015). Endothelial cells control pancreatic cell fate at defined stages through EGFL7 signaling. *Stem Cell Rep.* **4**, 181-189.

Kera, H., Yuki, S. and Nogawa, H. (2014). FGF7 signals are relayed to autocrine EGF family growth factors to induce branching morphogenesis of mouse salivary epithelium. *Dev. Dyn.* **243**, 552-559.

Knosp, W. M., Knox, S. M., Lombaert, I. M. A., Haddox, C. L., Patel, V. N. and Hoffman, M. P. (2015). Submandibular parasympathetic gangliogenesis requires sprouty-dependent Wnt signals from epithelial progenitors. *Dev. Cell* **32**, 667-677.

Knox, S. M., Lombaert, I. M. A., Reed, X., Vitale-Cross, L., Gutkind, J. S. and Hoffman, M. P. (2010). Parasympathetic innervation maintains epithelial progenitor cells during salivary organogenesis. *Science* **329**, 1645-1647.

Knox, S. M., Lombaert, I. M. A., Haddox, C. L., Abrams, S. R., Cotrim, A., Wilson, A. J. and Hoffman, M. P. (2013). Parasympathetic stimulation improves epithelial organ regeneration. *Nat. Commun.* **4**, 1494.

Kwon, H. R. and Larsen, M. (2015). The contribution of specific cell subpopulations to submandibular salivary gland branching morphogenesis. *Curr. Opin. Genet. Dev.* **32**, 47-54.

Lammert, E., Cleaver, O. and Melton, D. (2001). Induction of pancreatic differentiation by signals from blood vessels. *Science* **294**, 564-567.

Laresgoiti, U., Nikolić, M. Z., Rao, C., Brady, J. L., Richardson, R. V., Batchen, E. J., Chapman, K. E. and Rawlins, E. L. (2016). Lung epithelial tip progenitors integrate glucocorticoid- and STAT3-mediated signals to control progeny fate. *Development* **143**, 3686-3699.

Larsen, M., Hoffman, M. P., Sakai, T., Neibaur, J. C., Mitchell, J. M. and Yamada, K. M. (2003). Role of PI 3-kinase and PIP3 in submandibular gland branching morphogenesis. *Dev. Biol.* **255**, 178-191.

Larsen, M., Bogdanov, P., Sood, R., Kwon, H. R., Nelson, D. A., Duffy, C., Peters, S. B. and Chittur, S. V. (2017). Systems biology: salivary gland development, disease, and regenerative medicine (in Press). In *Salivary Gland Development and Regenerative Medicine: Advances in Research and Clinical Approaches to Functional Restoration* (ed. S. Cha). Switzerland: Springer (in press).

Lazarus, A., Del-Moral, P. M., Ilovich, O., Mishani, E., Warburton, D. and Keshet, E. (2011). A perfusion-independent role of blood vessels in determining branching stereotypy of lung airways. *Development* **138**, 2359-2368.

Lin, R.-Z., Moreno-Luna, R., Li, D., Jaminet, S.-C., Greene, A. K. and Melero-Martin, J. M. (2014). Human endothelial colony-forming cells serve as trophic mediators for mesenchymal stem cell engraftment via paracrine signaling. *Proc. Natl. Acad. Sci. USA* **111**, 10137-10142.

Lombaert, I. M. A., Brunsting, J. F., Wierenga, P. K., Faber, H., Stokman, M. A., Kok, T., Visser, W. H., Kampinga, H. H., de Haan, G. and Coppes, R. P. (2008). Rescue of salivary gland function after stem cell transplantation in irradiated glands. *PLoS ONE* **3**, e2063.

Lombaert, I. M. A., Abrams, S. R., Li, L., Eswarakumar, V. P., Sethi, A. J., Witt, R. L. and Hoffman, M. P. (2013). Combined KIT and FGFR2b signaling regulates epithelial progenitor expansion during organogenesis. *Stem Cell Rep.* **1**, 604-619.

Magenheim, J., Ilovich, O., Lazarus, A., Klochendler, A., Ziv, O., Werman, R., Hija, A., Cleaver, O., Mishani, E., Keshet, E. et al. (2011). Blood vessels restrain pancreas branching, differentiation and growth. *Development* **138**, 4743-4752.

Maimets, M., Rocchi, C., Bron, R., Pringle, S., Kuipers, J., Giepmans, B. N. G., Vries, R. G. J., Clevers, H., de Haan, G., van Os, R. et al. (2016). Long-term in vitro expansion of salivary gland stem cells driven by Wnt signals. *Stem Cell Rep.* **6**, 150-162.

Marcelo, K. L., Goldie, L. C. and Hirschi, K. K. (2013). Regulation of endothelial cell differentiation and specification. *Circ. Res.* **112**, 1272-1287.

Matsumoto, K., Yoshitomi, H., Rossant, J. and Zaret, K. S. (2001). Liver organogenesis promoted by endothelial cells prior to vascular function. *Science* **294**, 559-563.

Matsumoto, S., Kurimoto, T., Taketo, M. M., Fujii, S. and Kikuchi, A. (2016). The WNT/MYB pathway suppresses KIT expression to control the timing of salivary proacinar differentiation and duct formation. *Development* **143**, 2311-2324.

Mattingly, A., Finley, J. K. and Knox, S. M. (2015). Salivary gland development and disease. *Wiley Interdiscip. Rev. Dev. Biol.* **4**, 573-590.

Minuzzo, S., Agnusdei, V., Pusceddu, I., Pinazza, M., Moserle, L., Masiero, M., Rossi, E., Crescenzi, M., Hoey, T., Ponzoni, M. et al. (2015). DLL4 regulates NOTCH signaling and growth of T acute lymphoblastic leukemia cells in NOD/SCID mice. *Carcinogenesis* **36**, 115-121.

Mouhieddine, O. B., Cazals, V., Kuto, E., Le Bouc, Y. and Clement, A. (1996). Glucocorticoid-induced growth arrest of lung alveolar epithelial cells is associated with increased production of insulin-like growth factor binding protein-2. *Endocrinology* **137**, 287-295.

Musselmann, K., Green, J. A., Sone, K., Hsu, J. C., Bothwell, I. R., Johnson, S. A., Harunaga, J. S., Wei, Z. and Yamada, K. M. (2011). Salivary gland gene expression atlas identifies a new regulator of branching morphogenesis. *J. Dent. Res.* **90**, 1078-1084.

Nedvetsky, P. I., Emmerson, E., Finley, J. K., Ettinger, A., Cruz-Pacheco, N., Prochazka, J., Haddox, C. L., Northrup, E., Hodges, C., Mostov, K. E. et al. (2014). Parasympathetic innervation regulates tubulogenesis in the developing salivary gland. *Dev. Cell* **30**, 449-462.

Nelson, D. A. and Larsen, M. (2015). Heterotypic control of basement membrane dynamics during branching morphogenesis. *Dev. Biol.* **401**, 103-109.

Nelson, D. A., Manhardt, C., Kamath, V., Sui, Y., Santamaria-Pang, A., Can, A., Bello, M., Corwin, A., Dinn, S. R., Lazare, M. et al. (2013). Quantitative single cell analysis of cell population dynamics during submandibular salivary gland development and differentiation. *Biol. Open* **2**, 439-447.

Patel, N., Sharpe, P. T. and Miletich, I. (2011). Coordination of epithelial branching and salivary gland lumen formation by Wnt and FGF signals. *Dev. Biol.* **358**, 156-167.

Patel, V. N., Lombaert, I. M. A., Cowherd, S. N., Shworak, N. W., Xu, Y., Liu, J. and Hoffman, M. P. (2014). Hs3st3-modified heparan sulfate controls KIT+ progenitor expansion by regulating 3-O-sulfotransferases. *Dev. Cell* **29**, 662-673.

Perri, A. F., Dallard, B. E., Baravalle, C., Licoff, N., Formía, N., Ortega, H. H., Becú-Villalobos, D., Mejia, M. E. and Lacau-Mengido, I. M. (2014). Cellular proliferation rate and insulin-like growth factor binding protein (IGFBP)-2 and IGFBP-3 and estradiol receptor alpha expression in the mammary gland of dairy heifers naturally infected with gastrointestinal nematodes during development. *J. Dairy Sci.* **97**, 4985-4996.

Peters, S. B., Nelson, D. A., Kwon, H. R., Koslow, M., DeSantis, K. A. and Larsen, M. (2015). TGFbeta signaling promotes matrix assembly during mechanosensitive embryonic salivary gland restoration. *Matrix. Biol.* **43**, 109-124.

Rafii, S., Butler, J. M. and Ding, B.-S. (2016). Angiocrine functions of organ-specific endothelial cells. *Nature* **529**, 316-325.

Ramasamy, S. K., Kusumbe, A. P. and Adams, R. H. (2015). Regulation of tissue morphogenesis by endothelial cell-derived signals. *Trends Cell Biol.* **25**, 148-157.

Remédio, L., Carvalho, T., Caiado, F., Bastos-Carvalho, A., Martins, D., Duarte, A., Yagita, H. and Dias, S. (2012). Context- and cell-dependent effects of Delta-like 4 targeting in the bone marrow microenvironment. *PLoS ONE* **7**, e52450.

Rocha, A. S., Vidal, V., Mertz, M., Kendall, T. J., Charlet, A., Okamoto, H. and Schedl, A. (2015). The angiocrine factor Rspondin3 is a key determinant of liver zonation. *Cell Rep.* **13**, 1757-1764.

Salvesen, G. S. and Dixit, V. M. (1997). Caspases: Intracellular signaling by proteolysis. *Cell* **91**, 443-446.

Schlieve, C. R., Mojica, S. G., Holoyda, K. A., Hou, X., Fowler, K. L. and Grikscheit, T. C. (2016). Vascular Endothelial Growth Factor (VEGF) bioavailability regulates angiogenesis and intestinal stem and progenitor cell proliferation during postnatal small intestinal development. *PLoS ONE* **11**, e0151396.

Schmidt, A., Brixius, K. and Bloch, W. (2007). Endothelial precursor cell migration during vasculogenesis. *Circ. Res.* **101**, 125-136.

Sequeira, S. J., Gervais, E. M., Ray, S. & Larsen, M. (2013). Genetic modification and recombination of salivary gland organ cultures. *J. Vis. Exp.* **71**, e50060.

Tucker, A. S. (2007). Salivary gland development. *Semin. Cell Dev. Biol.* **18**, 237-244.

Wei, C., Larsen, M., Hoffman, M. P. and Yamada, K. M. (2007). Self-organization and branching morphogenesis of primary salivary epithelial cells. *Tissue Eng.* **13**, 721-735.

Wells, K. L., Gaete, M., Matalova, E., Deutsch, D., Rice, D. and Tucker, A. S. (2013). Dynamic relationship of the epithelium and mesenchyme during salivary gland initiation: the role of Fgf10. *Biol. Open* **2**, 981-989.

Whittles, C. E., Pocock, T. M., Wedge, S. R., Kendrew, J., Hennequin, L. F., Harper, S. J. and Bates, D. O. (2002). ZM323881, a novel inhibitor of vascular endothelial growth factor-receptor-2 tyrosine kinase activity. *Microcirculation* **9**, 513-522.

Yamada, K. M. and Cukierman, E. (2007). Modeling tissue morphogenesis and cancer in 3D. *Cell* **130**, 601-610.

Yoshitomi, H. and Zaret, K. S. (2004). Endothelial cell interactions initiate dorsal pancreas development by selectively inducing the transcription factor Ptf1a. *Development* **131**, 807-817.

Zhang, J. Y., Cui, L., Xu, M. H. and Zheng, Y. L. (2014). Restoring the secretory function of irradiation-damaged salivary gland by administrating deferoxamine in mice. *PLoS ONE* **9**, e113721.

Zudaire, E., Gambardella, L. S., Kurcz, C. and Vermeren, S. (2011). A computational tool for quantitative analysis of vascular networks. *PLoS ONE* **6**, e27385.

Table 1. Antibodies for immunocytochemistry

Antigen	Source	Dilution
CD31/PECAM-1	557355, BD Pharmingen	1:100
Cleaved Caspase 3	9661, Cell Signaling	1:100
Collagen IV	AB769, Millipore	1:100
Cytokeratin 7	ab9021, Abcam	1:100
Cytokeratin 19	Troma-III-c, DSHB*	1:100
Kit/CD117	AF1356, R&D Systems	1:100
PDGFRβ	Ab32570, Abcam	1:100
Tubb3	MAB1195, R&D Systems	1:200
VEGFR2/KDR/FLK-1	MA5-115157, Thermo	1:100
	9698, Cell Signaling	1:100

* DSHB, Developmental Studies Hybridoma Bank

Supplementary Table 2. Normalized intensities* of duplicative protein spots in mouse angiogenesis proteome array for conditioned media derived from 4 different explantly cultured tissues, including intact mesenchyme, CD31-depleted mesenchyme, CD31-depleted mesenchyme plus E12.5 CD31-positive endothelial cells, and CD31-depleted mesenchyme plus E16 CD31-positive endothelial cells (for Figure 5A).

		Array1	Array2	Array3	Array4
Protein Name	Spot	Intact mes	CD31-dep mes	CD31-dep+CD31pos(E12.5)	CD31-dep+CD31pos(E16)
ADAMTS1	A5	0.007962567	0.006192637	0.008330188	0.008283028
	A6	0.004203846	0.00499863	0.00944093	0.005938212
Amphiregulin	A7	-0.001999311	0.000605204	5.76949E-05	0.005113205
	A8	0.000298509	-0.003783117	0.003656831	0.003138102
Angiogenin	A9	0.005145998	0.002193285	0.005193503	0.001580635
	A10	0.000302539	-0.001377107	0.002198108	-0.006267225
Angiopoientin-1	A11	0.015521445	0.018830031	0.018927316	0.012647147
	A12	0.012182689	0.017420597	0.0174982	0.011813257
Angiopoientin-3	A13	0.001663635	0.001768534	0.001585669	-0.000179692
	A14	-0.002544395	0.004087773	0.000275483	0.001538085
Coagulation Factor III	A15	0.005668509	-0.001069857	0.000507043	0.003020236
	A16	0.005931591	0.003203805	0.001821522	0.006067566
CXCL16	A17	0.003173659	0.006000415	0.001085358	0.005399093
	A18	-0.003294677	0.006154014	0.005437999	0.004652166
Cyr61, IGFBP10	B3	0.007035463	0.009647633	0.009968283	0.014567731
	B4	0.003973333	0.011432303	0.009037693	0.013041327
DLL4	B5	0.001268985	0.002155766	0.00335156	0.007129741
	B6	-0.001462236	0.001505064	0.004113874	0.001564998
DPPIV	B7	0.000111744	-0.000996557	0.000308714	-0.002103149
	B8	0.006357199	0.000865359	0.00318557	0.000667973
EGF	B9	-0.004167283	-0.002463348	0.001352492	-0.001564615
	B10	-0.007136864	-0.001182517	-0.00445575	-0.00776528
Endoglin	B11	-0.003054221	0.002519215	-0.002541991	-0.005086387
	B12	-0.000283874	-0.002432407	-0.006012105	-0.002216547
Endostatin/Col18	B13	0.159248867	0.013255438	0.027347287	0.043492344
	B14	0.141765409	0.011860737	0.027766861	0.043310971
Endothelin-1	B15	0.009754054	0.010982767	0.012495372	0.013609593
	B16	0.018330758	0.011401625	0.009444666	0.013296526
FGF acidic, FGF1	B17	0.021190752	0.015364933	0.006455738	0.014800059
	B18	0.021181562	0.010635263	0.010205809	0.017326088
FGF basic, FGF2	B19	0.016169665	0.021034874	0.021895948	0.027158413
	B20	0.017929282	0.022023662	0.021335977	0.025840933
FGF7/KGF	C3	0.004683575	0.011432987	0.006313835	0.004757639
	C4	0.004258559	0.006560032	0.001605463	0.003934494
Fractalikine/CX3CL1	C5	-0.000524007	0.002289475	0.00125999	-0.000100494
	C6	0.000522465	0.00436103	-0.002108756	0.001709192
GM-CSF	C7	-0.000129464	-0.004502647	-0.007641836	-0.007504284
	C8	0.005087792	-0.002616157	-0.003299454	-0.002287979
HB-EGF	C9	-0.002801941	-0.000804125	-0.000283038	0.00093865
	C10	-0.006259313	0.002983694	-0.003448048	-0.000185224
HGF	C11	-0.001623955	0.005114395	0.001199884	0.003659349
	C12	-0.002675533	0.002195705	-0.002935693	0.004612967
IGFBP-1	C13	0.003797156	0.007275931	0.00022742	0.00318645
	C14	0.003767435	0.004725794	0.00309725	0.003306816
IGFBP-2	C15	0.588991245	0.216398646	0.482874357	0.508860367
	C16	0.603881176	0.209796746	0.499951045	0.524656562
IGFBP-3	C17	0.649047899	0.051114947	0.373683482	0.408900029
	C18	0.647317681	0.041559892	0.370478606	0.400454436
IL-1alpha	C19	0.002219683	-0.006417184	0.006518632	0.006137562
	C20	0.000382512	0.005580926	0.004540808	0.00098503
IL-1beta	C21	-0.005169953	0.002272584	-0.002323645	-0.001911457
	C22	-0.003282208	0.004830614	0.009202846	-0.000378511
IL-10	D3	0.008451809	0.018371972	0.015464283	0.013932394
	D4	0.007154025	0.013745122	0.017043554	0.012827084
IP-10, CXCL10	D5	0.001578879	0.008629167	0.005688796	0.019755102
	D6	0.003092396	-1.71805E-06	0.00240296	0.014786177
KC, CXCL1, GROalpha	D7	-0.004597406	-0.003210188	-0.004610867	0.009992082
	D8	-0.000135376	-0.004812528	-0.000339465	0.009799699
Leptin	D9	0.004258505	0.009325544	0.002820694	0.003165175
	D10	0.000352039	0.006521672	0.002761535	-0.00188465
MCP-1/CCL2/JE	D11	0.016665034	0.011394837	0.036671029	0.318284596
	D12	0.013141449	0.011374999	0.032124799	0.339797707
MIP-1alpha/CCL3	D13	-0.001464655	0.007163429	0.008359684	0.012982341
	D14	0.002980606	0.001847412	0.009297633	0.012128186

MMP-3(pro and mature)	D15	0.003257609	-0.000343276	0.003850142	0.001679619
	D16	0.001670246	-0.003718973	0.006434885	0.00137219
MMP-8	D17	0.007423288	-0.002202614	0.005751801	0.002481277
	D18	0.006075682	-6.93351E-05	0.006011408	0.002336285
MMP-9(Pro and Active)	D19	0.00334688	0.010993081	0.202978158	0.214364798
	D20	0.000711379	0.012456557	0.223864689	0.203652894
IGFBP-9/NOV/CCN3	D21	0.007447043	0.014137301	0.011348556	0.042714622
	D22	0.006243904	0.015366511	0.018896705	0.037853882
Osteopontin/OPN	E3	0.385456815	0.460502014	0.720151543	0.717194565
	E4	0.37937711	0.458505442	0.711606174	0.71400203
PD-ECGF	E5	0.006328822	0.007893799	0.011659849	0.014098821
	E6	0.003158933	0.00418933	0.00533535	0.002605419
PDGF-AA	E7	0.005807279	0.011987184	-0.00171366	0.004674825
	E8	0.004192936	0.008977356	-0.001501224	0.008699069
PDGF-AB/PDGF-BB	E9	0.000406751	0.006010203	-0.000346211	0.001328149
	E10	-0.000343638	0.002831674	-0.000213676	-0.001817261
Pentraxin-3	E11	0.003823277	0.012930613	0.003410049	0.009608167
	E12	0.006897553	0.013645828	0.00232345	0.005688651
CXCL4	E13	7.8261E-05	0.00258157	-0.001769585	0.005875396
	E14	0.00074986	0.004277153	-0.000568237	0.00715474
PIGF-2	E15	0.229157866	0.009574491	0.192283399	0.013906917
	E16	0.225925311	0.006945318	0.191472688	0.011175473
Prolactin	E17	0.002327764	0.000722969	0.003812227	-0.002488872
	E18	-0.003689543	0.000431873	0.004927987	0.003476753
Proliferin	E19	0.004517718	0.000465182	0.007192125	-0.001612697
	E20	-8.63066E-05	-0.002546541	7.59276E-05	-0.004310632
SDF-1/CXCL12	F3	0.118810427	0.038077271	0.319912055	0.468001632
	F4	0.108199469	0.029459488	0.315911744	0.465549162
Serpin E1/PAI-1	F5	0.00424093	-0.003354841	0.019215749	0.029237606
	F6	0.004289032	0.000895247	0.014818056	0.025147461
Serpin F1/PEDF	F7	0.007396845	-0.00291825	0.003372747	0.001702437
	F8	0.00869436	0.000198502	-0.000609888	0.004062412
Thrombospondin-2/TSP-2	F9	0.007004936	0.002165606	0.008204009	0.007196227
	F10	0.002756758	-0.003710343	0.005190046	0.003888007
TIMP-1	F11	0.00626508	0.001226282	0.01189771	0.007157453
	F12	0.006287115	0.005979472	0.008360408	0.006401856
TIMP-4	F13	-0.007300894	-0.000829172	-0.00150128	-0.002615833
	F14	0.0019401	-0.001243452	0.002876842	-0.007129518
VEGF	F15	0.003036931	-0.008114241	0.004256557	-0.005722841
	F16	0.004478107	-0.005751537	0.00314654	-0.005256697
VEGF-B	F17	0.003550896	0.002667236	0.004328595	0.000861899
	F18	-0.002027474	0.001257275	0.004631692	-0.004586787

* Normalized intensity = individual spot intensity / (positive reference intensity in the same array - negative reference intensity in the same array)

Supplementary Table 3. Normalized intensities* of duplicative protein spots in mouse angiogenesis proteome array for cell lysates derived from in vivo E13 epithelium and E13 mesenchyme tissue (for Supplementary Figure 3A).

		Array5	Array6
Protein Name	Spot	E13 Epi	E13 Mes
ADAMTS1	A5	0.027625936	0.08115729
	A6	0.031205419	0.076777969
Amphiregulin	A7	0.00856377	0.019225218
	A8	0.005239965	0.018716652
Angiogenin	A9	0.005580868	0.020242351
	A10	0.00856377	0.024480403
Angiopoientin-1	A11	0.059074249	0.07172056
	A12	0.050494854	0.06635236
Angiopoientin-3	A13	0.024813486	0.038748513
	A14	0.028932732	0.032165405
Coagulation Factor III	A15	0.009614888	0.017671266
	A16	0.01018306	0.017897295
CXCL16	A17	0.005012696	0.012500842
	A18	0.006291083	0.008997385
Cyr61, IGFBP10	B3	0.046205156	0.066465375
	B4	0.045296081	0.066973941
DLL4	B5	0.025239615	0.029311783
	B6	0.03160314	0.039002796
DPPIV	B7	0.018904498	0.032984761
	B8	0.02251239	0.034143162
EGF	B9	0.000126418	0.006595822
	B10	0.00555246	0.007302164
Endoglin	B11	0.004018396	0.029142261
	B12	0.003507041	0.029283529
Endostatin/Col18	B13	0.109300642	0.209429007
	B14	0.115948253	0.206066819
Endothelin-1	B15	0.035949654	0.042082447
	B16	0.029699764	0.047224617
FGF acidic, FGF1	B17	0.145067061	0.089944185
	B18	0.143334137	0.083163301
FGF basic, FGF2	B19	0.158078197	0.24497214
	B20	0.185662941	0.221126032
FGF7/KGF	C3	0.018307918	0.028803216
	C4	0.019955616	0.027644815
Fractalikine/CX3CL1	C5	0.01745566	0.020496634
	C6	0.019359036	0.017077938
GM-CSF	C7	0.005268374	0.009760235
	C8	0.002626374	0.009788488
HB-EGF	C9	0.018023832	0.016851909
	C10	0.013989812	0.021570274
HGF	C11	0.019841982	0.033888879
	C12	0.020296519	0.026853712
IGFBP-1	C13	0.029358861	0.043043072
	C14	0.032228129	0.035527593
IGFBP-2	C15	0.022682841	0.13142059
	C16	0.018393144	0.125402556
IGFBP-3	C17	0.008308093	0.191939978
	C18	0.014444349	0.173603338
IL-1alpha	C19	0.021603315	0.019422994
	C20	0.032114494	0.022785182
IL-1beta	C21	0.002938869	0.003035858
	C22	-0.000839474	-0.004027562
IL-10	D3	0.042483631	0.03044193
	D4	0.034046279	0.029114007
IP-10, CXCL10	D5	0.025495292	0.024367388
	D6	0.020324928	0.024960716
KC, CXCL1, GROalpha	D7	0.002825235	0.004363781

	D8	0.001717299	0.010833874
Leptin	D9	0.031574731	0.02829465
	D10	0.032625849	0.030498437
MCP-1/CCL2/JE	D11	0.016603402	0.023576285
	D12	0.028705463	0.026853712
MIP-1alpha/CCL3	D13	0.020040842	0.023632793
	D14	0.016972714	0.022050586
MMP-3(pro and mature)	D15	0.004984288	0.002470785
	D16	-0.001464463	0.002442531
MMP-8	D17	0.022626024	0.03419967
	D18	0.022086261	0.03504728
MMP-9(Pro and Active)	D19	0.018847681	0.019422994
	D20	0.01887609	0.016117313
IGFBP-9/NOV/CCN3	D21	0.027199808	0.014365585
	D22	0.025722561	0.017360475
Osteopontin/OPN	E3	0.023876002	0.019733784
	E4	0.028279334	0.024113105
PD-ECGF	E5	0.032256537	0.0183211
	E6	0.025211206	0.019112203
PDGF-AA	E7	0.03401787	0.030583198
	E8	0.032114494	0.037335828
PDGF-AB/PDGF-BB	E9	0.028705463	0.026486414
	E10	0.026887313	0.027164503
Pentraxin-3	E11	0.045807436	0.052677578
	E12	0.046489242	0.058497836
CXCL4	E13	0.021461272	0.19295711
	E14	0.021518089	0.18888858
PIGF-2	E15	0.013052328	0.012952901
	E16	0.01140463	0.015184942
Prolactin	E17	0.022228304	0.018236339
	E18	0.017342026	0.019366487
Proliferin	E19	0.019103359	0.025328013
	E20	0.023364647	0.020129336
SDF-1/CXCL12	F3	0.078931856	0.117322003
	F4	0.078818221	0.110371597
Serpin E1/PAI-1	F5	0.028591829	0.028859724
	F6	0.027796388	0.02292645
Serpin F1/PEDF	F7	0.040324578	0.041517373
	F8	0.042852942	0.039596123
Thrombospondin-2/TSP-	F9	0.018478369	0.013687496
	F10	0.02413168	0.015891284
TIMP-1	F11	0.017285209	0.019762038
	F12	0.01583637	0.021570274
TIMP-4	F13	0.019046541	0.02775783
	F14	0.016148865	0.01939474
VEGF	F15	0.012569382	0.007386925
	F16	0.008989899	0.00964722
VEGF-B	F17	0.043250663	0.054598828
	F18	0.03765417	0.046603036

* Normalized intensity = individual spot intensity / (positive reference intensity in the same array - negative reference intensity in the same array)

Supplementary Table 4. Normalized intensities* of duplicative protein spots in mouse angiogenesis proteome array for cell lysates derived from in vivo E12/E13 CD31-depleted mesenchyme and E12/E13 CD31-positive endothelial cells (for Supplementary Figure 3B).

		Array7	Array8
Protein Name	Spot	E12/E13 CD31-dep mes	E12/E13 CD31-positive cel
ADAMTS1	A5	0.145346216	0.121915424
	A6	0.138044596	0.121697055
Amphiregulin	A7	0.044695777	0.053702401
	A8	0.045095501	0.048789098
Angiogenin	A9	0.049545758	0.049635278
	A10	0.047786974	0.053101886
Angiopoientin-1	A11	0.133167966	0.125409328
	A12	0.119683952	0.12835731
Angiopoientin-3	A13	0.10372165	0.066285916
	A14	0.09945793	0.071499476
Coagulation Factor III	A15	0.073342645	0.0748569
	A16	0.087359625	0.068551495
CXCL16	A17	0.055514966	0.056513902
	A18	0.09748596	0.04264747
Cyr61, IGFBP10	B3	0.190221869	0.109987016
	B4	0.193846031	0.10946839
DLL4	B5	0.068599257	0.06238257
	B6	0.059512204	0.059216219
DPPIV	B7	0.088825279	0.043329873
	B8	0.077792903	0.04870721
EGF	B9	0.007921192	0.019500353
	B10	0.004376975	0.012921987
Endoglin	B11	0.014263476	0.183031453
	B12	0.009813218	0.17290459
Endostatin/Col18	B13	0.210501187	0.265957089
	B14	0.207489935	0.270160692
Endothelin-1	B15	0.125546567	0.092026164
	B16	0.120083676	0.090442989
FGF acidic, FGF1	B17	0.167650801	0.096229768
	B18	0.170288978	0.090579469
FGF basic, FGF2	B19	0.315628532	0.190838146
	B20	0.329645512	0.214039854
FGF7/KGF	C3	0.066440749	0.050809012
	C4	0.073982203	0.053484032
Fractalikine/CX3CL1	C5	0.048426532	0.044257941
	C6	0.042936992	0.042238028
GM-CSF	C7	0.006055815	0.01360439
	C8	-0.000206524	0.012212287
HB-EGF	C9	0.054582278	0.04483116
	C10	0.041924359	0.041992363
HGF	C11	0.064069054	0.055804203
	C12	0.057939957	0.051491415
IGFBP-1	C13	0.078032737	0.059270811
	C14	0.088692037	0.056568495
IGFBP-2	C15	0.23938789	0.06456626
	C16	0.239174704	0.069315786
IGFBP-3	C17	0.208769051	0.146563827
	C18	0.194938609	0.147874041
IL-1alpha	C19	0.07829922	0.057769524
	C20	0.068226181	0.061099652
IL-1beta	C21	-0.002418329	-0.001381184
	C22	-0.011265548	-0.003128136
IL-10	D3	0.083868704	0.063392527
	D4	0.071717102	0.067022911
IP-10, CXCL10	D5	0.102442534	0.038252793
	D6	0.106066696	0.038143609
KC, CXCL1, GROalpha	D7	0.004083844	0.012867395

	D8	0.004163789	0.012949283
Leptin	D9	0.074195389	0.057496563
	D10	0.066494045	0.055749611
MCP-1/CCL2/JE	D11	0.06931876	0.066204028
	D12	0.057273751	0.050754419
MIP-1alpha/CCL3	D13	0.047920215	0.044285237
	D14	0.044509239	0.044803864
MMP-3(pro and mature)	D15	-0.004097168	0.004214522
	D16	-0.002578218	0.002904308
MMP-8	D17	0.082269809	0.071008146
	D18	0.073049515	0.060581025
MMP-9(Pro and Active)	D19	0.052130639	0.043602834
	D20	0.049572407	0.044394422
IGFBP-9/NOV/CCN3	D21	0.046054838	0.046223262
	D22	0.038993051	0.040354595
Osteopontin/OPN	E3	0.080804155	0.063801968
	E4	0.083842056	0.055067208
PD-ECGF	E5	0.050425151	0.051655192
	E6	0.053649589	0.041746697
PDGF-AA	E7	0.115153749	0.08007046
	E8	0.114007875	0.087140157
PDGF-AB/PDGF-BB	E9	0.076060767	0.064648148
	E10	0.062869883	0.056786864
Pentraxin-3	E11	0.195551519	0.143288292
	E12	0.190621593	0.137037478
CXCL4	E13	0.084641503	0.464318047
	E14	0.091783234	0.451925605
PIGF-2	E15	0.061617416	0.050344978
	E16	0.073102811	0.047697253
Prolactin	E17	0.062843235	0.050072016
	E18	0.054662222	0.042019659
Proliferin	E19	0.080191246	0.069834413
	E20	0.075581098	0.072018103
SDF-1/CXCL12	F3	0.306541479	0.260607048
	F4	0.306408238	0.235057872
Serpin E1/PAI-1	F5	0.050105372	0.069943597
	F6	0.051970749	0.059025146
Serpin F1/PEDF	F7	0.100257378	0.085229429
	F8	0.101962866	0.077258959
Thrombospondin-2/TSP-	F9	0.018846975	0.026297089
	F10	0.015169516	0.021929709
TIMP-1	F11	0.095087617	0.079306169
	F12	0.085973916	0.069179306
TIMP-4	F13	0.031345004	0.031264984
	F14	0.033769995	0.028235114
VEGF	F15	0.015702481	0.008418126
	F16	0.008853881	0.009919413
VEGF-B	F17	0.104041429	0.05681416
	F18	0.100257378	0.051300342

* Normalized intensity = individual spot intensity / (positive reference intensity in the same array - negative reference intensity in the same array)

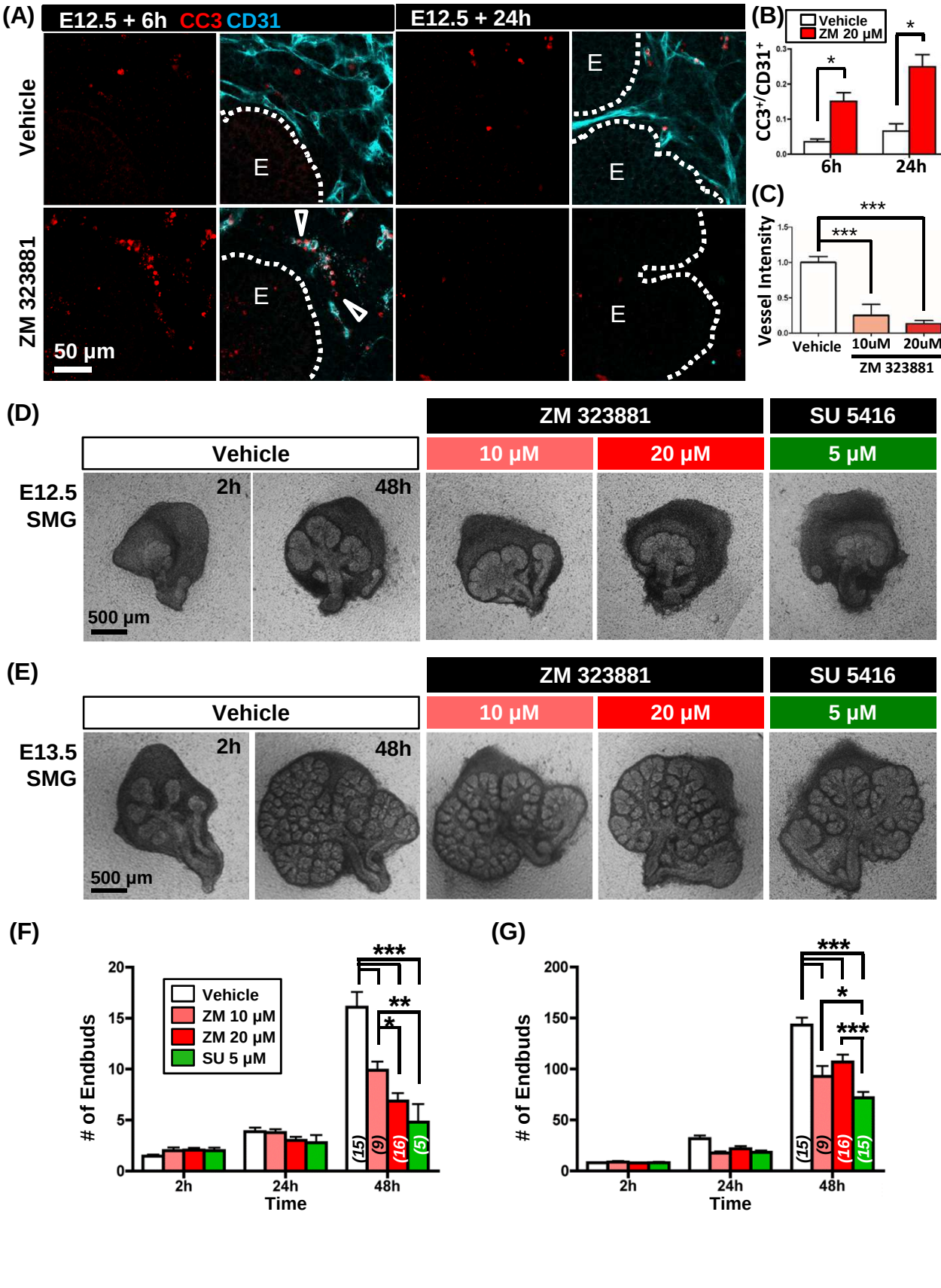

Supplementary Figure S1. VEGFR2 signaling promotes endothelial cell survival and early SMG epithelial patterning.

(A-C) VEGFR2 inhibition leads to increased SMG endothelial cell apoptosis. **(A)** ICC and confocal imaging of E12.5 SMGs cultured ex vivo for 6 or 24 hours +/- VEGFR2 inhibitor, ZM 323881 (20 μM) to examine the effect of VEGFR2 inhibition on endothelial cell apoptosis. VEGFR2 inhibition reduced $CD31^+$ vessels (cyan) in the mesenchyme even after 6 hrs, whereas it increased the level of cleaved caspase 3 (CC3, red) that overlapped with CD31 (white arrowheads). Most $CD31^+$ cells were not detectable by 24 hours. Dotted white lines indicate the boundary between the epithelial endbud (E) and the mesenchyme (M). Significant differences in $CC3^+$ cells were not detected in the mesenchyme, in general, or in the epithelium +/- ZM 323881 (data not shown). **(B)** Quantification shows areas co-positive for CC3 and CD31 were significantly increased in ZM 323881-treated glands relative to vehicle control. **(C)** Quantification shows total $CD31^+$ vessel intensity was significantly decreased with ZM 323881 in a dose-dependent manner. Brightfield images of **(D)** E12.5 and **(E)** E13.5 SMG cultured ex vivo for 48 hours in the absence or presence of VEGFR2 inhibitors both show reduced epithelial branching morphogenesis. Quantitative analyses of the **(F)** E12.5 and **(G)** E13.5 glands show that VEGFR2 inhibition reduced epithelial endbuds, revealing a conserved role of VEGFR2 signaling in promoting early SMG epithelial patterning. Error bars are shown as mean ± s.e.m. Student *t*-test for **(B-C)**, and two-way ANOVA **(F-G)** were performed for statistical analysis (* $p < 0.05$, ** $p < 0.01$, and *** $p < 0.001$)

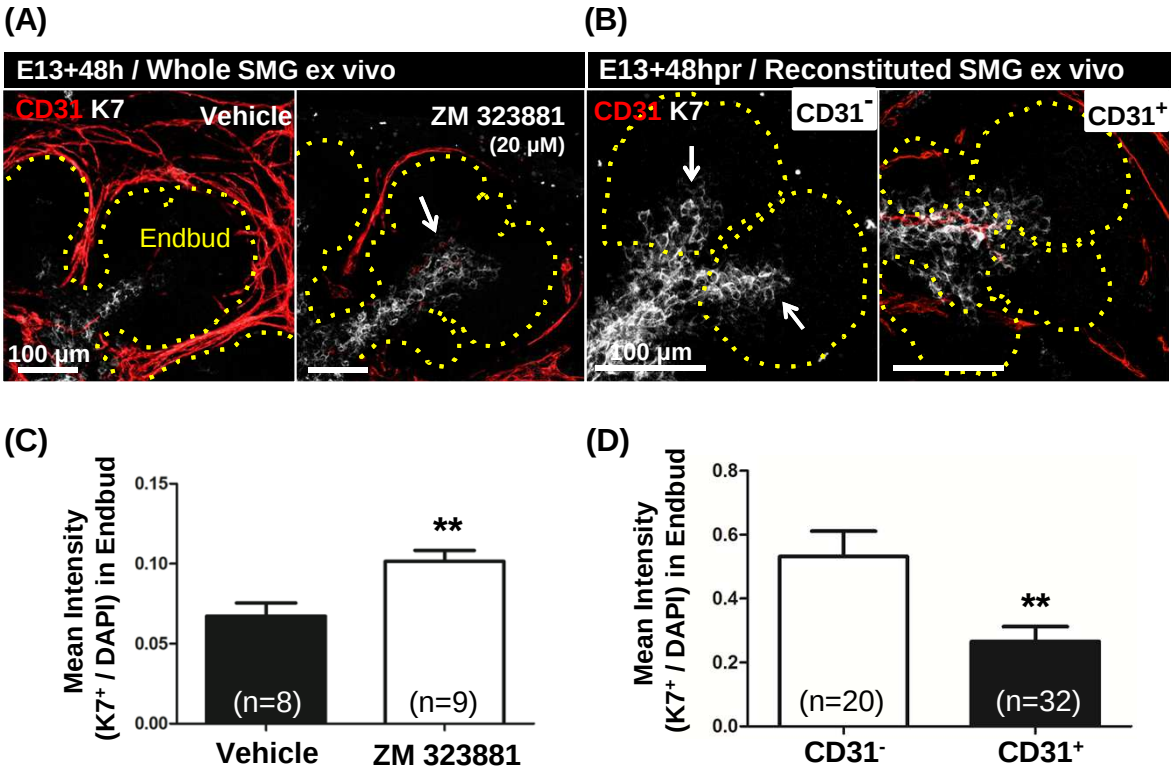

Supplementary Figure S2. Endothelial cells regulate SMG K7$^+$ duct cells in endbuds.
(A) ICC and confocal imaging of whole E13 SMGs cultured for 48 hours shows that VEGFR2 inhibition with ZM323881 (ZM) disrupted vascular development (CD31, red) and increased the presence of K7$^+$ ductal cells (white) inside the epithelial endbuds (white arrows) relative to controls. **(B)** ICC and confocal imaging of SMG cell fractionation/reconstitution assays cultured for 48 hours also shows increased K7$^+$ within the epithelial endbuds (white) of CD31 immuno-depleted and reconstituted glands (CD31$^-$) relative to CD31-supplemented glands (CD31$^+$). Quantification showed a significant difference in K7$^+$/DAPI intensity between **(C)** vehicle vs inhibitor treated glands and **(D)** endothelial-depleted vs endothelial-supplemented reconstituted glands. Dotted yellow lines indicate endbud boundaries. n = number of endbuds. Error bars are shown as mean ± s.e.m. Student *t*-test (** $p < 0.01$)

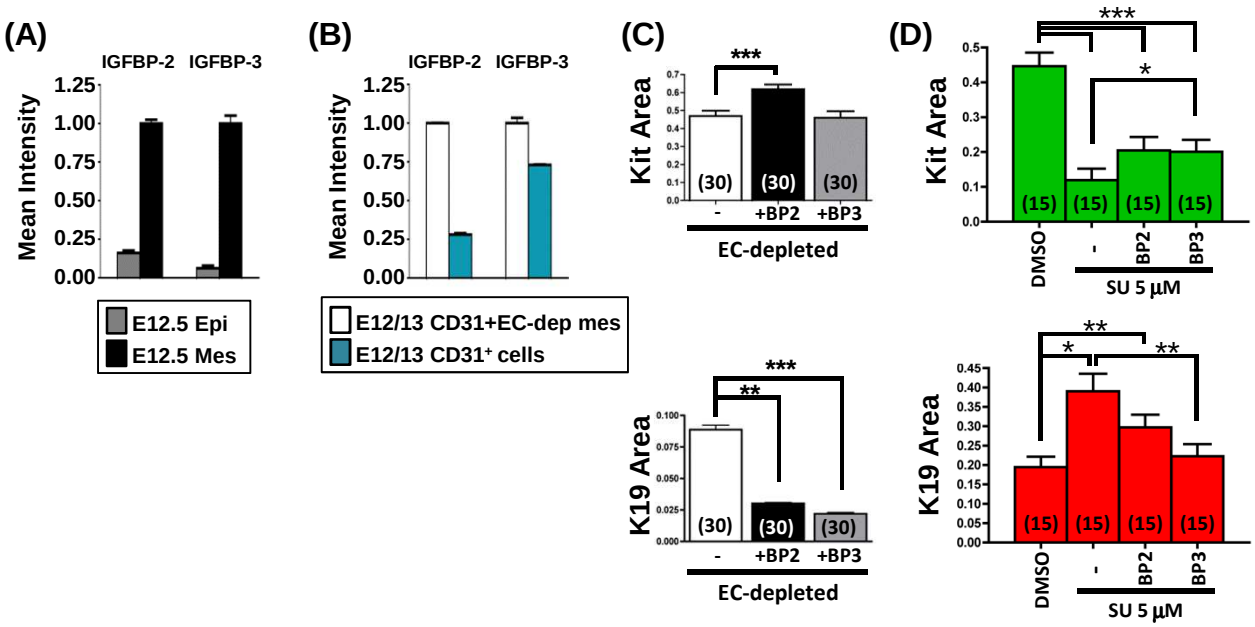

Supplementary Figure S3. IGFBP2 and IGFBP3 produced by the SMG mesenchyme regulate Kit and K19$^+$ progenitor cells.

(A) Cell lysates of freshly isolated E12.5 epithelium (Epi, gray) or mesenchyme (Mes, black) were analyzed with an angiogenesis proteome array. Mean intensity was normalized by mesenchymal intensity. IGFBP2 and IGFBP3 were primarily derived from mesenchyme. **(B)** Cell lysates of E12/13 CD31$^+$ endothelial cell immuno-depleted mesenchymal cells (E12/13 CD31$^+$ EC-dep mes) and E12/13 immuno-separated CD31$^+$ cells (E12/13 CD31$^+$ cells) were analyzed with an angiogenesis proteome array. Mean intensity was normalized by E12/13 EC-dep mes intensity. IGFBP2 and IGFBP3 were produced by both the CD31$^-$ and the CD31$^+$ mesenchymal cells. Full normalized data for the arrays shown in A and B are available in Tables S3 and S4, respectively. **(C, D)** IGFBP2 and IGFBP3 effects on Kit and K19 within endbuds. **(C)** ICC and confocal images (single sections through the middle of endbud) for Kit or K19 were individually quantified to measure Kit$^+$ or K19$^+$ cell area in epithelial endbuds of SMG cell fractionation/ reconstitution assay glands with CD31$^+$ endothelial depletion (EC-depleted) ± IGFBP2 (BP2) or IGFBP3 (BP3). Endbud Kit$^+$ expression area was significantly increased by addition of recombinant IGFBP2 but not IGFBP3. In contrast, K19$^+$ expression area was decreased by both IGFBP2 and IGFBP3.**(D)** ICC and confocal imaging (single section of the middle of endbud) of Kit or K19 were quantified to measure Kit$^+$ or K19$^+$ cell areas in endbuds of whole E13.5 glands treated with DMSO vehicle control or VEGFR2 inhibitor SU 5416 (SU, 5 µM) ± IGFBP2 or IGFBP3. Endbud Kit expression was decreased with with SU, and was partially rescued by addition of recombinant IGFBP2 and IGFBP3. Endbud K19 expression was increased by SU 5416 (5 µM), and partially restored to control levels by IGFBP2 but not IGFBP3. Error bars are shown as mean ± s.e.m. Student *t*-test was performed for statistical analysis (* $p < 0.05$, ** $p < 0.01$, and *** $p < 0.001$).